Electrochemical Measurement of Crevice Corrosion of Type AISI 304 Stainless Steel

A Thesis Submitted to the College of

Graduate Studies and Research

in Partial Fulfillment of the Requirements

for the Master of Science

in the Department of Chemical Engineering

University of Saskatchewan

Saskatoon

By

Aniekan Etor

Permission to Use

In presenting this thesis in partial fulfillment of the requirements for a Postgraduate degree from the University of Saskatchewan, I agree that the Libraries of this University may make it freely available for inspection. I further agree that permission for copying of this thesis in any manner, in whole or in part, for scholarly purposes may be granted by the professors who supervised my thesis work or, in their absence, by the Head of the Department or the Dean of the College in which my thesis work was done. It is understood that any copying or publication or use of this thesis or parts thereof for financial gain shall not be allowed without my written permission. It is also understood that due recognition shall be given to me and to the University of Saskatchewan in any scholarly use which may be made of any material in my thesis.

Requests for permission to copy or to make other uses of materials in this thesis in whole or part should be addressed to:

Head of the Department of Chemical Engineering

University of Saskatchewan

Saskatoon, Saskatchewan S7N 5A9

Canada

Abstract

Crevice corrosion is a form of galvanic corrosion that occurs when a metal is exposed to different environments. This occurs when the oxygen within the crevice gets depleted, thus acting as the anodic site for metal dissolution reaction. The anodic site thus encourages the migration of Cl^- ions into the crevice leading to the development of an aggressive local solution. The acidic conditions present in the crevice reaches a critical crevice solution composition and results in the loss of stability of the passive film which further leads to a rapid breakdown of these films on the metal thus indicating the onset of active corrosion.

In this research, it is hypothesized that the onset of crevice corrosion can be detected by measuring the galvanic coupling current between electrodes in a crevice and an external metal surface composed of the same material as the electrodes. To prove this hypothesis an engineered crevice was designed to measure IR controlled crevice currents along the crevice length of AISI 304 stainless steel immersed in a 0.5 M solution and a 1 M NaCl solution. Varying crevice openings were used to determine the effect of crevice gap (G) on the initiation of crevice corrosion and the position of the accelerated attack within the crevice.

Multiplexed corrosion potential measurement and galvanic corrosion measurement techniques were used to measure the change in the open circuit potential (OCP) and the galvanic current for the four channels along the crevice length of the galvanic couple. The results obtained from the MGC test for the 100 μm crevice width immersed in 0.5 M NaCl solution showed good results with high anodic current at approximately 1 cm from the crevice mouth. This finding was in close agreement with the peak pH value observed at the position closest to the crevice mouth in the work of Alavi and Cottis (1987) and the model prediction of Kennell *et al.* 2009. However, for test samples with crevice width ≥ 200 μm, there was no initiation of crevice corrosion and the results obtained were discarded. The Linear polarization resistance scan and Potentiodynamic polarization scan carried out along the crevice to measure the polarization resistance, R_p , and to obtain the region of passivity along an AISI 304 SS

crevice did not yield good results. Low corrosion rate in the range of 0.06 mm/yr was calculated for the AISI 304 stainless steel crevice.

Acknowledgements

My special appreciation goes to my supervisor, Dr. Richard Evitts, and to my co-supervisor, Dr. Aaron Phoenix, for their guidance, encouragements and professional assistance throughout my programme, and for making my stay in the Department of Chemical Engineering worthwhile.

I would like to thank my advisory committee members: Dr. Ike Oguocha, Dr Gordon Hill, and my External examiner, Dr. Ian Burgess.

I greatly appreciate the technical help of all the Engineering shops staff, Robert Peace, Rlee Prokopishyn, Kevin Carter, Unyime Umoh and Dragan Cekic who have contributed immensely to this research work in their various capacities. I would like to express my gratitude all the staff of the Department of Chemical Engineering, and to my colleagues Glyn Kennell, Jonathan Godwin, Cletus Asuquo, Bassey Bassey and Samuel Hanson for their encouragements during the period of this research work.

I will not fail to appreciate my friends like Tejumoluwa, Florence, Rosaria and Christiana. My daily interactions with you and all your encouragements have indeed registered a deep impression in me which I will ever cherish in my memory.

I owe my parents and siblings so much gratitude for their daily prayers and encouragements, and to my family friends in Calgary: Zik, Joanna, Ifedi, Nnadozie and Yagazie, thanks for all the love and attention, God bless!

Finally, to my husband and best friend, Williams Etuk Udofia, your daily encouragement, prayers, understanding and unwavering support has been a major source of strength to me. Thank you Koko for constantly believing in me, I deeply appreciate you.

Dedication

To God Almighty,

To My Parents

Dr. Robert Etor & Dr. (Mrs) Comfort Etor

And

My Siblings, Nsikak, Edidiong and Ikanke-Abasi

Table of Contents

List of Tables

List of Figures

List of Abbreviation and Symbols

b_a Tafel slope of anodic polarization curve (mV/decade)

b_c Tafel slope of cathodic polarization curve (mV/decade)

E Electrode potential (mV)

$E_{A/P}$ Active / passive potential (mV)

E_{surf} or E_{app} Applied potential (mV)

E_{rev} Reversible Potential (mV)

E_{corr} Corrosion Potential (mV)

E_{flade} Flade potential

F Faraday's Constant (96485 C/mol)

M_w Molecular weight (g/mol)

I Current (μA)

i_{corr} Anodic current density (μA/cm^2)

L Crevice depth (cm)

R_p Polarization resistance (Ω cm^2)

SS Stainless steel (AISI 304)

OCP Open circuit potential (mV)

MGC Multiplexed galvanic corrosion

LPR Linear polarization resistance

MPP Multiplexed potentiodynamic polarization

T Temperature (˚C)

t Time (h)

ZRA Zero Resistance Ammeter

HER Hydrogen Evolution Reaction

AISI American Institute of Steel and Iron

ASTM American Standard of Testing and Material

Greek Symbols

$\Delta\phi^*$ Difference between E_{app} and $E_{A/P}$

ρ Density (g/cm^3)

β_a, β_c Tafel constants ($\beta_a = b_a/2.303$, $\beta_c = b_c/2.303$)

1 Introduction

1.1 Overview

Corrosion is the destruction of a metal by electrochemical reactions with its environment. The economic impact of corrosion is far greater than most people realize. Millions of dollars are lost each year because of corrosion. The cost of corrosion in the US alone was $276 billion per year (NACE International, 2001). Of this amount, about $121 billion was spent to control corrosion, leaving the difference of $155 billion as the net loss to the economy. Utilities made with metal parts, such as water and sewer systems, suffer the largest economic impact from corrosion. This is mainly due to the destruction of the structural integrity of these systems (Betts and Boulton, 1993).

For corrosion to take place, four major components of the corrosion cell must be present, namely: the anode where oxidation occurs, the cathode where reduction takes place, an electrically conductive solution and the metallic path for electron transfer (Ahmad, 1994). For a metal in contact with an electrolyte, the metal may oxidize leading to the formation of a surface oxide film. The problem with some of these oxide films is that they do not firmly adhere to the surface of the metal, and they flake off easily causing structural weakness and disintegration of the metal over time (Kadgry, 2008).

In corrosion processes, the oxidation and reduction reactions can either occur evenly over the entire exposed metal surface, as in the case of uniform corrosion, or at

separate locations on the metal. In the latter case, corrosion initiation may occur at locations that are either occluded or isolated from oxygen, while the reduction reactions occur on the metal surface external to these occlusions (Alavi and Cottis, 1987). A typical example of localized corrosion is corrosion that occurs between joints such as crevice corrosion, or under a paint film as in filiform corrosion.

Stainless steel and its alloys are widely used in industrial systems due to their excellent corrosion resistance properties. However, they are more susceptible to localized corrosion than uniform corrosion in aggressive environments (Kabi, 1985). Some of the most common forms of localized corrosion are pitting corrosion, galvanic corrosion, stress corrosion cracking and crevice corrosion.

Crevice corrosion is a form of localized attack that occurs frequently on metals exposed to stagnant solutions within shielded areas such as holes, gaskets, lap joints and crevices under bolts. This form of corrosion is usually very difficult to detect, predict and design against due to the size and locations of the corroding crevice (Fontana and Greene, 1967). It can also be thought of as a galvanic process that occurs between different areas of an identical metal galvanic couple immersed in an electrolyte (Sun, 2000). This form of corrosion starts close to the crevice mouth and becomes more widespread, progressively moving to the interior of the material throughout the period of exposure to the aggressive solution. Materials with high corrosion resistance are usually the most vulnerable to this form of corrosion. Well known examples of susceptible metals are stainless steel alloys, nickel, titanium and aluminum (Kadry, 2008).

In spite of all the various studies involving other forms of localized corrosion, little understanding exists on the processes that occur during the onset of stainless steel crevice corrosion. The initiation of crevice corrosion that leads to the breakdown of the passive film in these localized areas on stainless steels is believed to result from a number of factors that are environmental, metallurgical, electrochemical and geometrical in nature (Lee, 1981), and understanding the mechanism of passive film formation and breakdown will help in achieving better corrosion protection of stainless steel alloys used in industrial systems. The influence of some of these factors on corrosion initiation is discussed in Chapter 2.

1.2 Mechanism of Crevice Corrosion

Various researchers have made attempts to examine the problems of crevice corrosion as well as propose mechanisms for its progression (Fontana and Greene, 1967; Kain, 1979; Oldfield and Sutton, 1978; Lee, 1981; Alavi and Cottis, 1985; Pickering, 1993; Wolfe, 2006; Bocher *et al*. 2008). The reproducibility of the results, namely, the corrosion initiation and propagation rate, has always been a problem in crevice corrosion studies. The crevice corrosion mechanism is complex due to its dependence upon many factors, and is included in the discussion of crevice corrosion initiation and propagation stages.

Given a metallic crevice in an oxygen - saturated electrolytic solution at neutral pH, metal dissolution and the accompanying cathodic oxygen reduction to hydroxide ions occurs uniformly over the metal surface including in the interior of the crevice.

These reactions are represented as in equation (1.1) and (1.2) during the initiation stage (Fontana and Greene, 1967).

Anodic Metal dissolution $M \rightarrow M^{n+} + ne^-$ ..... (1.1)

Cathodic Oxygen reduction $O_2 + 2H_2O + 4\,e^- \rightarrow 4OH^-$ ..... (1.2)

Eventually, the oxygen within the crevice gets depleted due to mass transfer limitations created by the crevice geometry, while the oxygen in the bulk solution does not deplete. This creates a differential aeration cell where the bold area external to the crevice acts as the cathodic site and the crevice area, with less or no oxygen, acts as the anodic site with metal dissolution. Furthermore, metal ions are transported slowly out of the crevice by diffusion or migration, and hydrolysis of these ions leads to a gradual pH decrease in the crevice as represented in equation (1.3).

$M^{n+} + 2H_2O \leftrightarrow M(OH)^{(n-1)+} + H_3O^+$ ..... (1.3)

The conduction of these charged metal ions through the electrolyte may cause a significant drop in potential, commonly referred to as the *IR* drop (Pickering *et al.* 1993). Electro-neutrality requires the migration of anions such as OH^- and Cl^- ions towards the crevice, but the OH^- precipitates as a metallic hydroxide, $M(OH)_n$ before reaching the crevice.

$2M^{n+} + 4OH^- \leftrightarrow 2M(OH)_n$ ..... (1.4)

The Cl^- ions are attracted to the anodic metal surface, and this lead to the development of an aggressive acid chloride local solution within the crevice.

At the end of the incubation phase of crevice corrosion, a high concentration of hydrogen ions have accumulated in the crevice due to hydrolysis of dissolution products, and there is a build up of chloride ions in the crevice. This may lead to the loss

of stability of the passive film protecting the metal. This facilitates anodic dissolution and leads to a more rapid breakdown of these films on the metal. However, the external area of the metal sample, where cathodic reactions occur, still remains passive during this process (Laycock *et al.* 1997; Betts and Boulton, 1993).

As dissolved species build up within the crevice, high anodic current is observed towards the mouth of the crevice as supported by the bold surface cathodic reactions. This increase in anodic current close to the crevice mouth is attributed to the lower IR drop between the crevice mouth and the bold surface. As the distance from the crevice mouth increases, larger IR drop is established between the crevice mouth and the crevice tip, and if the potential drop at the crevice tip becomes too large, the net anodic current produced at locations deeper into the crevice will cease due to mass transfer limitations (Betts and Boulton, 1993; Kennell *et al.* 2009). Finally, the accumulation of corrosion products at the crevice mouth over time may cause a significant decrease in the corrosion rate by introducing large resistance between the crevice and the external bold surface.

1.3 Knowledge Gap and Objectives

Most experimental and simulation studies on crevice corrosion have focussed on the galvanic contact between stainless steel and a dissimilar noble or active metal (Kabi, 1985, Simeos and Ferreira, 1987, Arai *et al.* 2002, Reclaru *et al.* 2002, Yin *et al.* 2008). These studies have been mostly designed to understand the active / passive transition behaviour during the crevice corrosion of these dissimilar metal systems. Crevice corrosion at specific positions in a crevice of AISI 316 stainless steel coupled to

dissimilar metals has been studied using Linear Polarization and Potentiodynamic Polarization techniques (Chang *et al.* 2000; Bocher *et al.* 2006, 2008; Fushimi *et al.* 2008). In addition, various researchers have simulated the pH profiles and current distribution during crevice corrosion of Titanium and Type 304 stainless steel (Postlethwaite *et al.* 1995; Evitts, 1997; Heppner *et al.* 2002; Kennell *et al.* 2008).

However, no information seems to be available on the galvanic current or the crevice corrosion behaviour of type AISI 304 stainless steel crevice coupled to an AISI 304 stainless steel bold surface. It is hypothesized that the onset of crevice corrosion can be detected by measuring the galvanic coupling current between electrodes in a crevice and an external metal surface composed of the same AISI 304 stainless steel material as the crevice material. To prove this hypothesis, an engineered crevice of AISI 304 stainless steel with four electrodes positioned along a line perpendicular to the crevice mouth was designed.

The main focus of this work was to provide information about the potential and current behaviours at each individual positions along the crevice assembly immersed in 0.5 M NaCl solution at room temperature (23 ± 1˚C), and pH of 6.5. The influence of varying electrolyte concentrations and crevice dimensions on the crevice corrosion of the AISI 304 stainless steel metal under both short term and long term exposures was studied. The study used an ECM8 Multiplexer galvanic corrosion measurement in the zero resistance ammeter mode (ZRA) to measure the galvanic current between the metal couple along four positions in the crevice. The corrosion potential of all four electrodes was also measured. This multiplexed mode allowed for the consecutive electrochemical measurements from different channels in one single scan.

The second phase of the study involved employing linear polarization resistance (LPR) to determine the corrosion rate, and the multiplexed potentiodynamic scan to determine the crevice corrosion resistance of the metal. Knowledge of the mechanism of this attack and long-term corrosion behaviour of type AISI stainless steel in various chloride concentrations will enhance the understanding of the crevice corrosion process in same metal galvanic couples.

1.4 Thesis Outline

This thesis is divided into five chapters. Chapter 1 gives an overview of crevice corrosion and the mechanism for crevice corrosion initiation including the role that *IR* drop and critical crevice solution play during the initiation process. The knowledge gaps found in the literature are reviewed and the objectives of the work are stated.

Chapter 2 presents the literature review, providing details on the process of crevice corrosion, the factors that influence this process, as well as experimental approaches for engineered crevice studies reported by various researchers.

Chapters 3 presents details on the sample preparation for the experimental work, the design of the crevice assembly as well as the experimental conditions employed for the study. In addition, details of the electrolyte preparation, the electrochemical measurement equipment used, and the electrochemical measurement techniques chosen for the experiments are documented in this section.

Chapter 4 covers the results and discussion of the experimental findings. The crevice corrosion rate obtained from the galvanic corrosion test is compared to the corrosion rate obtained from the linear polarization and potentiodynamic scan to assess

the effectiveness of the galvanic corrosion in providing information on the corrosion behaviour of the samples studied at different positions along the crevice.

Chapter 5 concludes this work and presents some recommendations for further studies to improve this research.

2 Literature Review

This chapter presents a brief overview of stainless steel alloys and their application in industrial systems. Crevice and galvanic corrosion behaviour of stainless steels and other alloys, and the factors that affect the protective film of these alloys are also presented in this section. Furthermore, theories governing crevice corrosion, experimental techniques used for previous studies and the experimental techniques to be used in this work are explained in detail.

2.1 Stainless Steel and Its Alloys

Stainless steels are high temperature steels with many industrial applications because of their remarkable resistance to corrosion due to a chromium-rich oxide film which forms on the surface (Kadry, 2008). The passive oxide film formed is usually very thin, and protective in oxidizing environments such as air and water. The corrosion resistance of stainless steel makes it one of the principal steels used in many commercial applications. However, when stainless steels are exposed to harsh environments, they become susceptible to localized corrosion that destroys the protective passive film. Therefore, care must be taken to select a grade of stainless steel which will be suitable for the environment (Kadry, 2008). The use of stainless steel and its alloys can be classified into a wide variety of general applications as shown in Table 2.1.

Stainless steels have been classified into several categories such as martensitic, ferritic, austenitic and duplex groups (ASM Specialty Handbook: Stainless steels, 1994; Sedrik, 1979). However, for the purpose of this work, emphasis will be placed on the AISI 304 stainless steel which is an austenitic stainless steel. The austenitic stainless steels are steel that contain 18-20 wt % nickel which gives the austenitic structure. AISI 304 stainless steel is a commercial grade of austenitic stainless steel that has been widely used in the past due to its affordability, and its ability to form protective oxide film on its surface for corrosion resistance in oxidizing environments. Due to its availability and affordability, it will be used in this work to study the galvanic and crevice corrosion behaviour of the metal in various corrosive environments. The galvanic current trend observed between the crevice and bold surface will provide knowledge of the crevice corrosion behaviour of AISI 304 stainless steel.

2.1.1 Austenitic Stainless steels

Austenitic stainless steels have an austenite, face - centered cubic (fcc) crystal structure, and are well known for their good mechanical properties and corrosion resistance characteristics. The most common austenitic alloys are the Fe-Cr-Ni steels, generally known as the 300 series. They are ductile, tough and, most importantly, easy to form and weld. They contain sufficient chromium to offer corrosion resistance together with nickel that ensures they maintain the austenite form at room temperature and below (Shrier, 1994; Shirazi, 1996). Common examples of austenitic stainless steel can be seen in Table 2.2.

Table 2.1 Applications of stainless steel and its alloys under different environments (Kadry, 2008).

Applications	Examples
Consumer goods	Domestic kitchenware and tableware, kitchen sinks, laundry equipment and electrical and electronic appliances.
Architecture, building & construction	Roofing and guttering, signage, curtain wall supports, bridges, barrier walls and decking.
Food and beverage industry	Beer and wine fermenters, fruit juice tanks and piping, storage vessels.
Transportation	Automotive exhaust systems, seagoing chemical tankers and passenger railcars.
Chemical	Heat exchangers, high temperature furnace equipment, and components for nuclear reactors.

Table 2.2 Typical chemical composition and mechanical properties of some austenitic stainless steel (Shirazi, 1996).

AISI type	% C	% Cr	% Ni	% Mo	% Other	0.2% Proof strength (MPa)	Tensile strength (MPa)	Tensile Elongation (%)	Hardness (HB)
304	**0.08**	**18-20**	**8-10**	**-**	**Mn, Si**	**205**	**515**	**40**	**201**
316	0.08	16-18	10-14	2-3	Si, Mn	205	515	40	217
316L	0.03	16-18	10-14	2-3	Si, Mn	170	485	40	217
347	0.03	17-19	9-13	-	Si, Cb	205	515	40	201

Type AISI 304, also known as type 18 – 8 stainless steel, is the most commonly used of the austenitic grades, containing approximately 18 wt % chromium and 8 wt % nickel. It is used for chemical processing equipment, for food, dairy, and beverage industries, for heat exchangers, and for chemicals industrial plants. Addition of molybdenum and nitrogen can increases the corrosion resistance of this group, particularly in marine and acidic environments. The corrosion behaviour of type AISI 304 stainless steel has been studied by various researchers (Alavi and Cottis, 1985; Dayal *et al*. 1983; Kabi, 1985; Alkire and Lott, 1985, Betts and Boulton, 1993). Crevice corrosion and stress corrosion cracking amongst others are the most common form of localized attack on AISI 304 stainless steel (Chung *et al*. 1999; Ling and Ma, 2009).

2.1.2 Corrosion Behaviour of Austenitic Stainless Steels

Austenitic stainless steel is known to exhibit active-passive behavior which is usually measured using electrochemical techniques outlined in section 2.6. Anodic polarization curves plotted from stainless steel corrosion potential and current measurements reveal both general and localized corrosion behavior of these steels (Sedriks, 1986). A typical stainless steel in sulphuric acid anodic polarization curve as reproduced from Sedriks (1986) is shown in Figure 2.1.

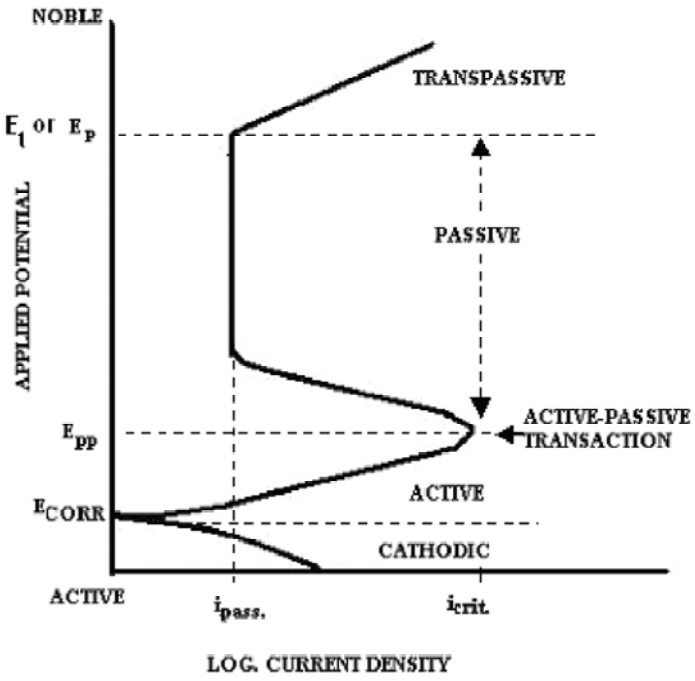

Figure 2.1 Anodic Polarization curve of stainless steel in sulphuric acid solution (Sedriks, 1986).

From the figure above, at potential values below the corrosion potential (E_{corr}), the metal is cathodic. As the potential is increased past the corrosion potential (E_{corr}), the metal becomes anodic and remains active in the potential region just above the corrosion potential (E_{corr}), and a bit below the passivation potential (E_{pp}). However, when the critical current density (i_{crit}) being the point of maximum anodic dissolution is reached by increasing $\Delta\phi^*$, the current density drops to a very low value, called the passive current density (i_{pass}). $\Delta\phi^*$ is the difference between the corrosion potential, E_{corr} and the active-passive potential on the polarization curve. This current drop is characterized by the formation of the protective oxide layer which is typically the self healing behavior of passive metals (Muwila, 2006). It is observed that during passivation, the metal still corrodes but at a significantly lower rate. When the applied

potential is at the transpassive region (E_T), the metal starts again to corrode at high rates and the extent to which the corrosion occurs is dependent on the aggressiveness of the corrodent (Alkire and Lott, 1985). The presence or absence of chloride ions determines the extent of passive film breakdown (Sedriks, 1986).

E_{corr} is known as the corrosion potential of the metal and is the location on the polarization curve where the total rate of all the anodic reactions equals the total rate of all cathodic reactions. The corrosion current at E_{corr} is called the corrosion current density, i_{corr}, and can be determined from the anodic polarization curve by the extrapolating the anodic and cathodic linear portions of the curves to the corrosion potential, E_{corr}, where under ideal conditions, they should intersect (Bard and Faulkner, 1980). Austenitic stainless steels are subject to different forms of corrosion depending upon the environment. The galvanic corrosion and crevice corrosion behaviour of austenitic stainless steel will be discussed in sections 2.1.2 and 2.1.3.

2.1.3 Galvanic Corrosion of Austenitic Stainless steels

Galvanic corrosion is the accelerated corrosion that occurs when two metals with different reduction potentials, are coupled electrically in a corrosive electrolyte (Reclaru *et al.* 2002). The tendency of any metal in a galvanic couple to corrode is dependent on its position in the galvanic series. The galvanic series is a list of metals and alloys ranked in order of their reduction potentials in a given environment (Ahmad, 1994). The reduction potential of a metal is the tendency of such metal to lose or gain electrons in reaction, and this potential is measured generally with respect to the standard calomel electrode (SCE). According to this series, when two metals are

coupled together, the electronegative member of the couple closer to the active region will corrode (anode), while the electropositive member of the couple closer to the noble region is protected (cathode).

The intensity of the galvanic corrosion process depends on a number of factors, such as the effective area ratio of the anodic and cathodic members, solution conductivity, the distance between the electrodes, temperature, pH and the stability of the protective films (Reclaru *et al.* 2002; Yin *et al.* 2008). The potential difference between two or more materials in a conductive medium was described by Luigi Galvani as the driving force for galvanic corrosion in the 18^{th} century (Ahmad, 1994).

However, studies carried out by Crues *et al.* (1997) show that the potential difference between a metal to metal couple in a conductive medium cannot provide a quantitative prediction of the galvanic damage. This was seen where a titanium/stainless steel couple showed lower galvanic current density in aerated 3 wt % NaCl solution than that recorded for the aluminum/stainless steel couple exposed in similar environment. It was expected that the titanium/steel couple, with greater potential difference between them based on the galvanic series, will experience severe galvanic corrosion than the aluminum/steel couple. The reduced galvanic corrosion behaviour of the titanium/steel couple was attributed to the low limiting current density of cathodic reduction of oxygen, due to the natural oxide film on the bare titanium metal. Also, the formation of a layer of corrosion product on the stainless steel greatly reduced the galvanic current density.

Reclaru *et al.* (2002) studied the galvanic corrosion behaviour of surgical implant CoCr alloy and REX 734 steel couples in 9g/l NaCl deaerated and non-

deaerated solutions. The study revealed low galvanic currents, i_g, in the range of nanoamperes generated by the galvanic couple. From the results, the cathode to anode area ratio of 1:1, nitrogen deaerated electrolyte, and oxygen controlled electrolyte at 0.2 mg/l were reported as the factors responsible for the low galvanic corrosion behaviour observed.

For metals that are close to each other in the series, their reduction potential range overlaps, and either of them can act as the anode or the cathode depending on the exposure conditions (Dexter and LaFontaine, 1998). For identical metal galvanic couple in a conductive medium, it is logical to say that, considering the galvanic series, no remarkable potential difference will exist between the metals and therefore little or no galvanic corrosion is expected to occur. However, depending on the nature of the exposed environment, and anode to cathode area ratio, galvanic corrosion can initiate in these systems.

In seawater environments, galvanic corrosion can occur in identical metal galvanic couple due to the increase in conductivity of the electrolyte. Also, small anode to large cathode area ratio will influence the rate of galvanic corrosion in a same metal couple. This is because the part of the metal couple with the small anode area displays a large current density, and hence, prone to greater damage during the corrosion processes (Ahmad, 1994).

2.1.4 Crevice Corrosion of Austenitic Stainless Steels

Crevice corrosion commonly occurs in austenitic stainless steel as well as other alloys of stainless steel that develop a barrier or passivation layer, and for this phenomenon to occur, three conditions must exist. First, the metal must be electrically connected to the external metal outside the crevice. Secondly, the solution in the crevice must be stagnant and provide an ionic path to the solution near the metal outside the crevice. Thirdly, the external metal surface must be passive (Fontana and Greene, 1967, Klassen *et al*. 2001).

When these conditions are met, differential aeration cells may be set up where the oxygen in the crevice gets depleted, causing the crevice to become the anodic site for metal dissolution reaction. Metal ion hydrolysis occurs within the crevice, and chloride ion migration into the crevice results in acidic chloride conditions within the crevice. At this stage, the crevice solution causes the loss of stability and the rapid breakdown of the protective passive layer in the crevice (Alavi and Cottis, 1985; Alkire and Lott, 1985).

Crevice corrosion can also be seen as a form of galvanic corrosion that occurs when two or more metals are exposed to different environments. For example, two similar metals, i.e. AISI 304 stainless steel crevice coupled in a conductive medium, can form a galvanic cell and generate an electric current. In such case, the galvanic current, i_g, will be generated as a result of the dissimilar electrolyte environments existing between the crevice solution and the bulk solution. The extent of crevice corrosion between dissimilar and similar metal couples depends on factors such as area ratio of

cathode to anode, temperature, pH and oxygen content of the solution to mention a few. These factors will be discussed in details in section 2.3.

2.2 Theories Governing Crevice Corrosion

Two basic crevice corrosion theories have been proposed: Critical Crevice Solution Theory (Oldfield and Sutton, 1978) and IR drop Theory (Pickering, 1986; Pickering *et al.* 1993; Pickering *et al.* 1998; Pickering, 2003; Eun-Young, 2005; Wolfe, 2006). Both mechanisms attempt to provide an explanation for the initiation and propagation of crevice corrosion of passive metals in contact with an electrolyte. However, of the two proposed mechanisms, IR voltage drop mechanism receives more attention as the ruling mechanism especially for active / passive metal alloys. The reason for the theory's success is that its mechanism provides an understanding for corrosion processes in both chloride-containing and chloride-free environments unlike the Critical Crevice Solution Theory (CCST).

The first theory to address the onset of crevice corrosion was the Acidification Mechanism or the Critical Crevice Solution Theory. It was developed by Oldfield and Sutton (1978). It proposes that the change in the chemical composition of the electrolyte and the formation of a critical crevice solution with high concentrations of hydrogen ions and chloride ions are responsible for the breakdown of the passive films on the metal surfaces.

The theory considers the influence of crevice geometry (i.e. the width and depth of the crevice gap) on mass transport of dissolved ions into and out of the crevice leading to the development of a critical crevice solution. Because of the changes in local

chemistry within the crevice, the depassivation of the passive film on the alloy will occur. When a low pH and a high chloride ion concentration in the crevice solution causes disruption of the passive film, the solution is said to have reached a critical state and thus active crevice corrosion will begin as observed by high rates of corrosion occurring in the crevice. This mechanism of localized corrosion relies on acidification (hydrolysis of metal ions) and the mass transport of dissolved ions i.e. chloride ions in and out of the crevice, but completely excludes the electrode potential, E, and its distribution, E_x, within the local cell. However, it takes into account the current generated in the crevice due to the mass transport of ions in and out of the crevice. Thus, a mechanism was proposed to account for the potential distribution within the crevice during the onset of crevice corrosion.

The IR drop mechanism was developed by Pickering (1986). According to this mechanism, crevice corrosion progression results from an IR voltage drop in the crevice solution which creates a localized electrode potential on the crevice wall within the active peak region of the polarization curve. Therefore, crevice corrosion would abruptly start when the potential difference between the crevice mouth and the interior was large enough to cause anodic sites to become active (Pickering *et al.* 1993). This potential difference is called the *IR* drop in the solution where I is the ionic current flowing out of the crevice or pit, and R is the resistance of the crevice/pit electrolyte (Kennell *et al*. 2008).

For active metal dissolution to occur in the crevice, the $IR > \Delta\phi^*$ criterion must be met, where $\Delta\phi^*$ is the difference between the corrosion potential, $E_{corr,}$ and the electrode potential of the active/passive transition, $E_{A/P}$. A decreasing magnitude of $\Delta\phi^*$

and an increasing magnitude of the ionic current, I, account for the passive current density and size of the active peak in the anodic polarization curve obtained during the potential-current measurement (Pickering *et al.* 1993; Pickering, 2003). The existence of the IR drop inside the crevice has been reported in iron, steel and nickel (Pickering *et al.* 1998; Abdusalem 2005, 2007).

Furthermore, crevice corrosion initiation can be described on the basis of the IR drop mechanism as the "immediate" type that requires no induction period or the "delayed form" that occurs after an induction period (Pickering, 2003, Kennell *et al*. 2009). Immediate crevice corrosion occurs when there is low IR drop between an anodic and cathodic site, leading to high rates of metal dissolution at the anodic region closest to the cathodic site (Pickering *et al.* 1998). Thus, when $IR > \Delta\phi^*$ is met, crevice corrosion occurs immediately on the part of the crevice wall that was in the active peak region of polarization, ($L>L_c$), where the crevice length, L, is greater than the system's critical crevice length, L_c. However, in principle, a decrease in I or R and/or increase in $\Delta\phi^*$ could cause a switch of $IR > \Delta\phi^*$ to $IR < \Delta\phi^*$ causing immediate termination of crevice corrosion (Pickering *et al.* 1993). Furthermore, Pickering *et al.* (1998) showed that a gradual increase in pH and Ni^{2+} ion concentrations during stagnation of the crevice electrolyte caused a termination of crevice corrosion process.

For the delayed crevice corrosion to occur, the $IR < \Delta\phi^*$ condition must be met. However, if this condition is not met, the role of other factors such as change in temperature, electrolyte composition, corrosion product accumulation, mass transport and acidification may influence the incubation period causing this condition to be met

(Pickering, 1986; Pickering *et al.* 1993, 1998, 2003). For corrosion to occur, high level of hydrogen and chloride ions build up in the crevice will force the $IR < \Delta\phi^*$ condition during the incubation period to switch to $IR > \Delta\phi^*$, causing the anodic sites to become active (Pickering *et al.* 1993, 1998, 2003; Kennell *et al*. 2009).

2.3 Factors Affecting Crevice Corrosion

There are several factors that are responsible for crevice corrosion initiation in stainless steel alloys. Such factors can be environmental in nature and they include bulk and crevice solution oxygen content, pH, chloride level and temperature (Fontana and Greene, 1978). Furthermore, alloy composition, mass transport in and out of a crevice, metal dissolution and passive film characteristics are factors that also can influence crevice corrosion (Lee and Kain, 1983). Geometrical aspects such as the exterior to interior crevice area ratio, width and depth of the crevice are also known to contribute to this phenomenon (Fontana and Greene, 1978, Kennell *et al.* 2009).

2.3.1 Temperature and pH Effects

During the corrosion process, increase in temperature accelerates the reaction kinetics of metal dissolution and reduction reactions causing the breakdown of the passive region. In essence, an increase in temperature causes an increase in the conductivity of electrolytes thus leading to a corresponding increase in the rate of electrochemical reaction and anodic current (Pickering *et al.* 1998; Jones, 1996).

However, Lee (1981) studied the effect of temperature on crevice corrosion initiation and propagation in 5 different crevice specimens of AISI 304 and 316 stainless steels immersed in naturally aerated seawater for 28 days at 10, 25 and 50°C. Visual observation of initiation times and gravimetrically determined propagation rates were obtained and the corrosion currents were calculated. It was observed that more corrosion was seen at 25°C than at 10 or 50°C after 28 days of exposure. The higher corrosion rates at 25°C can be attributed to acceleration in the reaction kinetics of the dissolution and reduction reactions, as well as to an increase in mass transport of species into the crevice. However, at a higher temperature of 50°C, oxygen solubility is reduced, thereby decreasing the external cathodic reaction rate, which in turn lowers the rate of corrosion. The molybdenum–free type 304 stainless steel samples exhibited faster corrosion initiation than type 316 alloys.

A similar observation was documented by Kain (1979) for the same alloys. Based on Kain's result, an increase in temperature of the test environment from 10°C to 28°C to 50°C increased the extent of crevice corrosion initiation and severity of attack on stainless steel alloys in ferric chloride solutions. A drop in the corrosion rate at 50°C was observed compared to the corrosion rate of 28°C and 10°C. Lee and Kain (1983) and Kain (1985) reported that sample surface finish, duration of exposure, relative crevice tightness as well as bulk environment chloride level affect the ultimate crevice electrolyte pH and chloride level during the initiation and propagation stages of crevice corrosion. It was observed that increase in any of the above listed factors increased the initiation and propagation of crevice corrosion spontaneously.

Pickering *et al.* (1993) observed a low pH and a sharp decrease in electrode potential due to acidification and chloride build up in the crevice during active stages of crevice corrosion. Also, at increased temperature, an increase in the anodic peak current density and a shift in the potential of the active/passive transition, E_{pass}, towards the noble (more positive) direction was observed for iron in an acetate buffer (Pickering *et al.* 1998).

It is known (Pickering, 1986) that, in principle, crevice corrosion will occur when the IR drop is large enough to satisfy the $IR > \Delta\phi^*$ criterion for the initiation and stabilization of crevice corrosion. Based on this criterion, Wolfe *et al*. (2006) reported the effect of increase in resistance, *R*, and decrease in pH in the crevice in promoting the switch of $IR < \Delta\phi^*$ to $IR > \Delta\phi^*$ in the delayed form of crevice corrosion. A decrease in the crevice pH occurred until the equilibrium hydrolysis pH was reached, causing an active peak to be formed in the polarization curve of the crevice during the induction period.

2.3.2 Crevice Geometry Effects

Crevice geometry is another very important factor in crevice corrosion susceptibility. The presence of sufficiently tight crevices favours the setting up of the differential aeration cavities and the differential concentration of protons (Oldfield and Sutton, 1978). The nucleation and propagation of the phenomenon is associated with the creation and development of localized solutions within the crevice different to the general solution. Oldfield and Sutton (1978) showed that crevice corrosion initiation

time in seawater increased as the crevice gap dimension increased from 0.1 μm to 1 μm. Furthermore, Kain (1983 and 1985), in a similar study proposed that for a crevice depth of 0.1 cm, a gap of less than 0.01 μm might be required for initiation of crevice corrosion of type 304 stainless steel in natural waters with 1000mg/l chloride ion content.

Previous studies (Dayal *et al.* 1983; Alavi and Cottis, 1987; Chang *et al*. 2000) also showed that crevice corrosion initiation time is strongly dependent on the depth/width ratio of the crevice geometry. An increase in crevice gap width consequently increases the time of initiation. A wider crevice gap reduces the chloride ion activity in the crevice of AISI 304 stainless steel thereby increasing the corrosion initiation time (Alavi and Cottis, 1987). Based on these observations, it was explained that tighter crevices would be necessary for crevice corrosion to initiate at lower chloride levels due to oxygen diffusion restrictions.

Kennell *et al.* 2009 used critical crevice corrosion scaling laws to model crevices dimensions that will become active upon oxygen depletion, become active after an incubation period or not become active at all. The crevice lengths modeled were between 1 cm and 8 cm, and the crevice widths between 1 μm to 1 mm. The corrosion processes were modeled for extended period of time for specific length and width during each simulation. From the model, immediate crevice corrosion was observed for crevice length above 1 cm with crevice width of $\leq$ 100 μm. For the crevice length above 1 cm and crevice width > 100 μm, the crevice became active after a period of incubation, and crevice length below 1 cm for all crevice width did not become active.

The critical aspect ratio, AR_c, was observed at the boundary between the active crevice zone and the not-active crevice zone, where the crevice scaling factor, $L^2/G = 401$ cm.

However, in contrast to expectation, Pickering (2003) observed that crevice corrosion will occur faster in a crevice of large opening / gap dimension, a = 0.05 cm and applied potential >350 mV. It was predicted that the wider gap creates less IR drop in the crevice electrolyte than a tighter gap, thus more chances of crevice corrosion initiation. A similar view was presented by Abdusalem (2007). He observed that for a crevice gap of 300 μm, an application of E_{surf} = 530 mV on nickel in various sulphuric acid solutions caused the initiation of crevice corrosion at varying depth inside the crevice. In addition, work by Pickering *et al.* (1998) shows 400 μm as the upper limit crevice width for crevice corrosion initiation in a 1N Sulphuric acid solution.

Alkire and Lott (1985) reported that no crevice corrosion was observed for type 304 stainless steel in 0.1 N NaCl solutions with large crevice gaps of > 7.5 μm, low manganese sulphide inclusion densities and an applied potential of < 75 mV. However, with tighter crevice of ≤ 7.5 μm, higher inclusion densities and applied potentials of ≥ 75 mV, crevice corrosion was observed to occur. They therefore inferred that crevice corrosion did initiate due to pit formation through dissolution of the manganese sulphide inclusions.

Eun-Young Na *et al.* (2005) investigated the initiation of crevice corrosion for ferritic stainless steel by measuring the potentials and current change in the crevice using a depth profile technique with a micro capillary tube. The measured potentials at various crevice widths were lower than the external surface potential of the metal due to the IR drop between the opening and bottom of the crevice. The crevice corrosion

developing time for 0.1 mm and 0.2 mm widths were 15 mins and 23 mins respectively. However, the larger crevice width of 0.5 mm showed no evidence of crevice corrosion initiation. This supports the view that crevice corrosion will not initiate in crevice widths larger than 0.4 mm (Pickering *et al.* 1998).

2.3.3 Alloy Composition

It is well known that the presence or absence of certain alloying elements in stainless steel results in higher or lower crevice corrosion initiation and propagation resistance, and the influence of these elements vary with temperature and pH. Stainless steels containing relatively high levels of molybdenum, nickel and chromium, which are elements that are known to increase resistance to depassivation, are less prone to localized corrosion (Trasatti and Mazza, 1996). Therefore, they generally require very low pH and high chloride ion concentration to cause a breakdown of their passive film (Betts and Boulton, 1993). A rise in the critical crevice potential in the noble direction, which is the lowest potential beyond which crevice corrosion can take place, through the presence of the molybdenum ions accounts for the difficulty in the film breakdown (Dayal *et al*. 1983; Trasatti and Mazza, 1996). The adsorbed MoO_4^{2-} ions at the active surface sites spontaneously repairs the passive film destroyed by localized attack through inhibitory actions (Arai *et al.* 2002).

The beneficial effect of chromium ions on passive films is noticed by the shift of the corrosion potential of the sample in the noble direction during the crevice corrosion initiation step (Alavi and Cottis, 1985; Betts and Boulton, 1993; Trasatti and Mazza, 1996). However, once corrosion occurs, the hydrolysis of chromium ions with metal ion

hydrolysis causes the localized crevice pH to fall to very low values typically in the range of 0-2 (Szklarska-Smialowska, 1986). Therefore, the synergistic action of chromium and other alloys in the passive films will produce better crevice corrosion resistance.

The presence of dissolved nickel ions also increases the difficulty of passive film breakdown by raising the critical crevice potential in the noble direction. These ions are less likely to contribute to the acidification of the solution within the crevice because hydrolysis of Ni^{2+} yield less acidic pH values (Dayal *et al*. 1983). Pickering, (1986) also found that increasing nickel content increases the corrosion resistance by shifting the potential of the metal in the noble direction.

It is expected that low or non-molybdenum bearing alloys will display a lower crevice corrosion resistance than molybdenum bearing alloys. However, their resistance to corrosion varies with different test environments. It was reported that a high nickel alloy Inconel 625 underwent IR- induced crevice corrosion initiation after a period of 18-20 days for tests conducted in a seawater environment. The same alloy was observed to demonstrate a significantly higher level of resistance to crevice corrosion when exposed to a chloride-thiosulphate environment (Shaw *et. al*. 1991; Mulford and Tromans, 1988).

The addition of elements such as sulphur and manganese decreases the corrosion resistance of metals (Muwila, 2006). Alloys with a high manganese content exhibit lower crevice corrosion resistance than those with a reduced content of <1 wt %. This is because the presence of manganese ions causes localized attack to occur at sulphide inclusions (Trasatti and Mazza, 1996). Copper ions increase the resistance of alloys to

passive film breakdown. However, after film breakdown, the presence of copper ions in the crevice promotes the initiation of crevice attack due to the galvanic effect of copper and the metal ions in the crevice electrolyte (Trasatti and Mazza, 1996).

The addition of nitrogen to austenitic stainless steels decreases i_{pass} and i_{crit} thus making passive film formation easier. The synergistic action of nitrogen and molybdenum in stainless steels significantly improves crevice corrosion resistance in these metals (Sedriks, 1986). It is suggested that nitrogen and molybdenum interact to form a protective film layer on the surface of the steel. The formation of molybdenum nitrides helps retain the molybdenum ion in the passive film by acting as an inhibitor to the dissolution of molybdenum in the transpassive region (Jargelius-Patterson, 1999; Muwila, 2006).

2.3.4 Passive Film Characteristics

The resistance of stainless steels to localized corrosion is a function of the thickness and composition of the passive film on the metal surface. Stainless steels exhibit a non-continuous, porous oxide film usually 1-5 nm thick which provides resistance to localized corrosion on the metal surface (Shrier, 1994). These films provide a barrier to oxidation reaction of the metal surface due to their low ionic conductivity.

It has been shown that a passive film consists of two layers, an inner oxide layer and an outer hydroxide layer (Borex and Olefjord, 1985; Shirazi, 1996). The interaction of passive films with an aqueous solution accounts for the formation of the outer hydroxide layer, while the inner layer of the passive film contains oxides and

hydroxides of the alloys present in the metal matrix (Shreir, 1994). The stability of passive film formed on austenitic steels is dependent on alloy composition, temperature, and the exposed environment (Muwila, 2006). The presence of chromium and molybdenum in the oxide enhances crevice corrosion resistance of stainless steel alloys.

The presence of chromium in the passive film shifts the corrosion potential in the noble direction, and reduces the active/passive current density. Consequently, if the chromium content in the passive film is <12 wt %, the passive film can be susceptible to localized corrosion. The presence of a high chloride level in the test environment can accelerate the breakdown of the passive film on a metal surface (Eun-Young Na *et al.* 2005).

2.3.5 Oxidant Availability

The initiation of crevice corrosion in narrow geometries is dependent on the occurrence of anodic dissolution in the crevice, with the corresponding cathodic reduction on the bold surface. A typical example of cathodic reduction is the reduction of oxygen, hydrogen ion reduction under acidic conditions or the reduction of water in neutral of alkaline conditions (Betts and Boulton, 1993). The relevant reduction reactions required for crevice corrosion initiation and their corresponding equilibrium potentials are summarized in Table 2.3.

The amount of oxidant and/or its availability to the bold surface drives the anodic dissolution reaction in the crevice, which in turn increases the rate of crevice corrosion. Therefore, a decrease in crevice corrosion susceptibility can be attributed to the decrease in the cathodic kinetics such as the availability of oxygen at the bold

surface (Betts and Boulton, 1993). In addition, the presence of these oxidants in the crevice electrolyte can suppress the anodic current on the crevice wall. This behaviour can be experienced in the presence of large crevice geometries which causes the $IR > \Delta\phi^*$ criterion for corrosion initiation to be less favourable (Pickering *et al.* 1998).

Table 2.3 Some reduction reactions required for crevice corrosion (after Bett and Boulton, 1993).

Type	Reaction	Equilibrium potential, (V_{SHE}) at 25˚C
Oxygen reduction (acidic conditions)	$O_2 + 4H^+ + 4e^- \rightarrow 2H_2O$	$E = 1.228 - 0.0591pH + 0.0148 \log P_{O2}$
Oxygen reduction (neutral/alkaline conditions)	$O_2 + 2H_2O + 4e^- \rightarrow 4OH^-$	$E = 0.401 - 0.0148pH - 0.0591 \log [OH^-]$
Hydrogen discharge evolution	$2H^+ + 2e^- \rightarrow H_2$	$E = 0.000 - 0.0591 \log [OH^-] - 0.0295 \log P_{H2}$
Hydrogen reduction (neutral/alkaline conditions)	$2H_2O + 2e^- \rightarrow H_2 + 2OH^-$	$E = -0.828 - 0.0591 \log [OH^-] - 0.0295 \log P_{H2}$

2.4 Engineered Crevice Studies

Single crevices have been fabricated by various researchers such as Alavi and Cottis (1987), Pickering *et al.* (1993, 1998, and 2003), Klassen *et al.* (2001), Abdusalem (2005, 2007), Wolfe *et al.* (2006) and Bocher *et al.* (2008). The results obtained show

significant variances in the crevice solution composition possibly arising from differences in the crevice geometry and experimental procedures.

2.4.1 The Artificial Crevice of Alavi and Cottis (1987)

Alavi and Cottis (1987) studied the potential, pH and chloride concentration variations in an engineered crevice of AISI 304 stainless steel (304 SS) and AA 7475 aluminum alloy, in 0.6 M bulk NaCl solutions. The crevice used in their experiment was built from a 304 SS plate with dimensions 80 mm long and 25 mm wide and encased in epoxy resin with a Perspex electrode holder as shown in Figure 2.2. The crevice gap was approximately 90 μm and the temperature of the electrolyte was set at 23 ± 1°C. pH values of 1-2 near the crevice mouth were measured for the 304 SS alloy and pH levels of 3-4 near the crevice mouth was measured for the AA 7475 aluminum alloy as well.

Furthermore, a pH of near 8 was measured around the crevice tip for both stainless steel and aluminum alloys. Results from the experiments show that the external potential dropped slowly to positive (noble) values as time and distance from the crevice mouth increased for both metals. This indicates that both crevices were subject to anodic dissolution, due to reduction in the oxygen concentration of the crevice electrolyte compared with the oxygen concentration in the bulk solution.

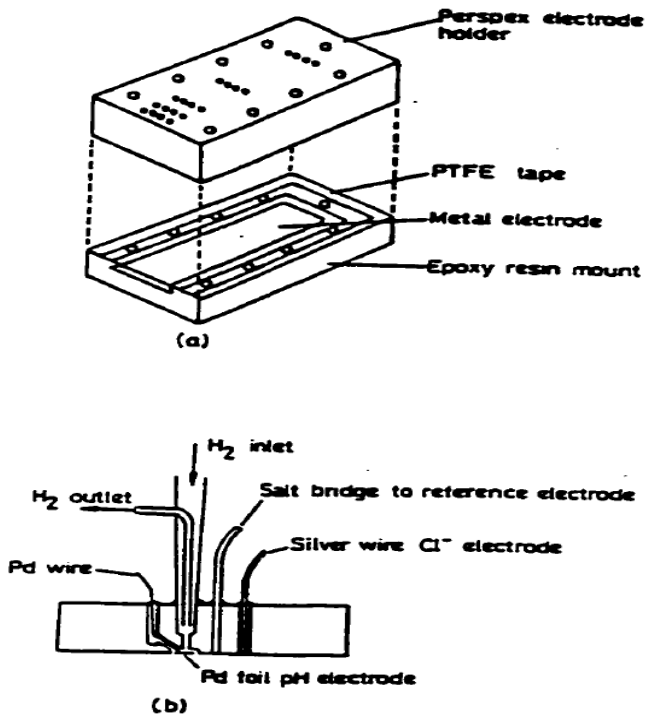

Figure 2.2 Schematic of artificial crevice design from Alavi and Cottis's experiment (1987).

2.4.2 The Artificial Crevice of Pickering *et al.* (1993 and 1998)

Previous works on crevice corrosion have established that an increase in chloride and hydrogen ions in the crevice promote the phenomenon (Fontana and Greene, 1967). However, an exception to this view was presented through the IR drop mechanism (Pickering, 1986; Pickering *et al.* 1993; 1998; 2003). This mechanism works such that neither the presence of the chloride ions nor acidification of the crevice electrolyte facilitates the occurrence of crevice corrosion.

The onset of crevice corrosion for pure iron in an alkaline solution (chloride-free) was studied (Pickering *et al.* 1993). The system design comprised of iron mounted in a Plexiglas plate to form a crevice. A fine Luggin capillary connected to a reference

electrode was inserted at different crevice locations in order to obtain the potential gradient from the top to the bottom of the crevice. It was proposed that crevice corrosion occurred when the IR drop in the crevice electrolyte was large enough for the electrode potential, E_x, at some distance into the crevice to be in the active region. This was observed in the absence of chloride build up and acidification in the crevice electrolyte. Furthermore, the behaviour of steel in 0.1 M H_2SO_4 indicated a steep potential gradient by the development of a horizontal boundary between the passivated upper and actively corroding lower parts of the crevice wall (Pickering *et al.* 1993).

Pickering *et al.* (1998) studied the effect of electrolyte properties on the crevice corrosion behaviour of iron in buffered chloride free solutions with pH range from 4.6 to 9.7. It was found that increasing the pH and solution conductivity of the crevice solution as well as decreasing the oxidant availability suppressed the metal's crevice corrosion susceptibility. It was further observed, that the increase in solution conductivity over time caused a decrease in resistance, R, along the crevice wall.

2.4.3 The Artificial Crevice of Klassen *et al.* (2001)

Klassen *et al.* (2001) designed a test apparatus that allowed direct measurement of the corrosion current between the test specimen and the counter electrode, and the corrosion potential versus a reference electrode. The crevice design was a modification to the gap crevice design found in the literature (Alavi and Cottis, 1985; Abdusalem, 2005). The gap crevice design has the crevice width parallel to the specimen surface, whereas, the crevice assembly designed for their study was such that the crevice was oriented perpendicular to the specimen surface by placing a crevice cover with a hole

over the specimen. The test specimens were made of nickel-aluminum-bronze material embedded in a cylindrical epoxy mount as one part of the crevice, and the other part of the crevice plate made from Perspex material. A conducting wire attached to the metal-epoxy block connected the Potentiostat to the metal sample. The electrolyte for their experiment was 3.5 wt % NaCl solution. A crevice hole of 0.18mm diameter was drilled into the crevice plates as shown in Figure 2.3.

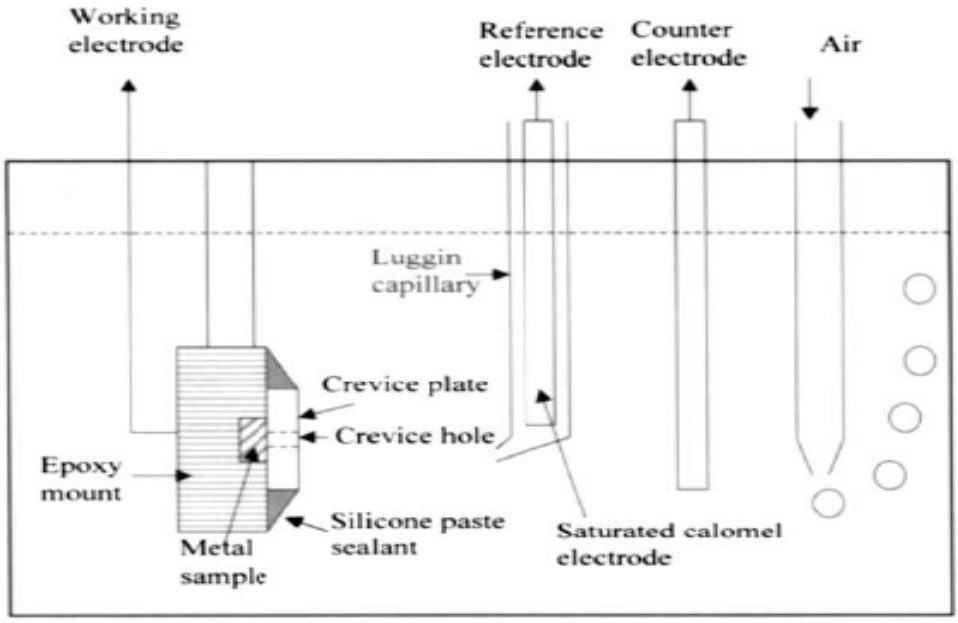

Figure 2.3 Schematic of the experimental crevice corrosion setup by Klassen *et al.* (2001).

A positive shift in the specimen potential that is consistent with an increase in the equilibrium potential of the controlling anodic reaction was observed for this crevice gap. A similar observation was reported by Alavi and Cottis, (1987).

2.4.4 The Inverted Crevice of Abdusalem (2005)

Abdusalem (2005) observed the current and potential gradient variations within a crevice made of low carbon steel and Plexiglas in a strong acetate solution with a reported bulk solution pH of 4.66. Figure 2.4 shows a schematic of their apparatus.

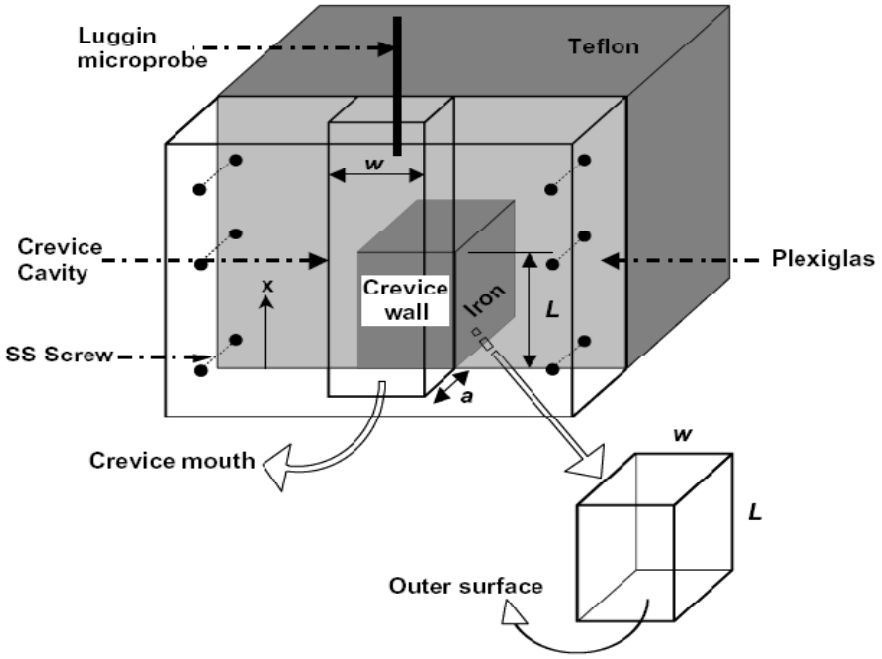

Figure 2.4 Schematic diagram of the crevice assembly used in the experiment (reproduced from Abdusalem, 2005).

The crevice assembly was placed in the electrolyte with the crevice mouth facing downward as seen in Figure 2.4 above. This downward orientation helps hold the pH constant due to convective mixing of the crevice solution and bulk solution, thus there was no measured pH variation during the experiment. It was observed that there was decay in the potential gradient with time as the crevice depth, L increased. Potential values below E_{pass}= -165 mV indicated the onset of active crevice corrosion. These results are in close agreement with the prediction of the IR drop theory (Pickering, *et al.* 1993; Abdusalem, 2007).

2.4.5 The Closed Crevice of Wolfe *et al.* (2006)

Wolfe *et al.* (2006) investigated the interaction of IR voltage, changes in pH, active peak formation and corrosion product accumulation during the induction period in delayed crevice corrosion of iron in 0.2 M $Na\,SO_4$ + 0.025 M $K_2\,Cr_2\,O_4$ with a pH of 9.1. A rectangular channel machined into a Plexiglas plate was placed against iron to form a crevice with an opening dimension of 0.06 cm, width of 0.5 cm, and depth of 11 mm as shown in Figure 2.5. A pH/electrode microprobe was positioned in the crevice to measure *in situ* pH and the local electrode potential along a distance, *x*, on the crevice wall.

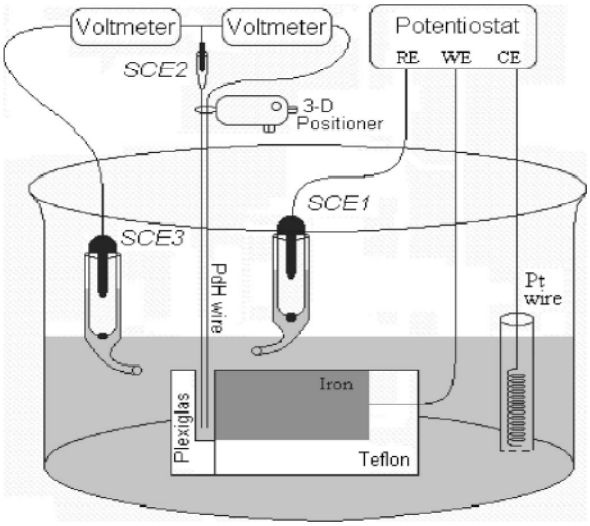

Figure 2.5 Schematic of crevice corrosion cell (reproduced from Wolfe *et al.* 2006).

A platinum wire counter electrode and a standard calomel reference electrode were used. The crevice opening faced upwards and the bottom of the crevice was closed to prevent the crevice from undergoing convective movement in and out of the crevice

from the bulk solution. It was observed that as the pH decreased in the crevice solution, an active peak was observed in the polarization curve for iron.

2.4.6 The Multiple Crevice Assembly of Bocher *et al.* (2008)

Bocher *et al.* (2008) monitored the anodic current evolution as a function of position during crevice corrosion initiation and propagation of AISI 316 and Alloy 625 stainless steel in an aerated 0.6 M NaCl solution at 50°C. The crevice assembly consisted of 100 wires of alloy 625 and 316 stainless steel respectively, each wire with diameter of 250 μm, inserted into a groove in a 2.54 cm AISI 316 stainless steel rod and polyformaldehyde (Delrin) in the case of alloy 625. Figure 2.6 displays the array of wires encased in an AISI 316 stainless steel rod.

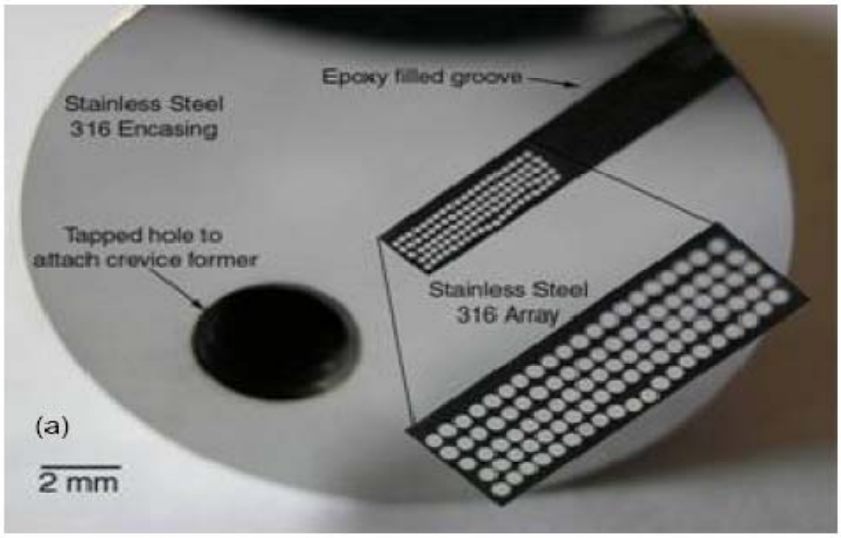

Figure 2.6 Close packed array of one hundred 250 μm diameter wires of AISI 316 stainless steel mounted in a 5*20 arrangement in AISI 316 stainless steel rod (reproduced from Bocher *et al.* 2008).

The arrays of wires were coated with a poly-imide film to ensure electrical insulation. The crevice was designed to cover 12 columns of 5 wires leaving remaining 8 columns open to bulk solution. The crevice array was immersed in the heated solution for 2 days at the open circuit potential to allow passive film stabilization and solution wicking into the whole crevice. Crevice corrosion was found to readily initiate close to crevice mouth at X_{crit} = 0 for 316 stainless steel. X_{crit} is the distance from the crevice mouth to the location where the potential reaches a critical passive potential value, E_{flade}, on the crevice wall. E_{flade} is defined as the lowest potential in the passive region below which marks a steep fall from the passive region to the active region.

However, crevice corrosion was observed to initiate further inside the crevice for Alloy 625, at the distance where the potential reached a critical passive potential value, E_{flade}, on the crevice wall. This was in agreement with the prediction that if the flade potential, E_{flade}, is greater than the applied potential $E_{app,}$ then crevice corrosion occurs at the mouth, but if the E_{flade} is less than E_{app} with a significant IR drop in the system, then crevice corrosion will initiate at a fixed distance from the crevice mouth (Scully, 2000).

2.5 Mathematical Models of Crevice Corrosion

Numerical models have been developed by many researchers to simulate the crevice corrosion processes and the transport phenomenon within the crevice. Oldfield and Sutton (1978) predicted that no concentration gradients existed in the crevice and mass transport occurred only between the bulk solution and crevice leading to the critical crevice solution during the incubation period of crevice solution of stainless

steels. The comparison of this model with experimental data showed reasonable agreement. The initiation period of aluminum crevice corrosion was modeled by Alkire and Siitari (1982). The results from pH, electrode potential, and current distribution showed that variations in the crevice geometry was found to have a significant effect on the current distribution behaviour during the initiation of crevice corrosion. Later, Herbert and Alkire (1983) made several improvements on the Alkire and Siitari (1982) model to achieve better agreement between the simulation and existing experimental data.

Walton *et al*. (1996) modelled the effect of the IR drop theory on the mass transport limitations in acidic solutions during crevice corrosion of stainless steel. The results showed that the passive current in the crevice was independent of the potential in the crevice, in approximate agreement to the Alavi and Cottis (1987) experiment. Evitts *et al.* (1993) determined the critical pH values of Inconel^{TM} 625 based on deoxygenation and acidification of the crevice. It was reported that the pH in the crevice was dependent on the temperature and chloride ion concentrations in the various systems. This finding was in agreement with Oldfield and Sutton (1978).

Evitts *et al.* (1996) numerically simulated the initial stages of stainless steel crevice corrosion to determine the accuracy of previous models using various passive current densities at elevated temperatures. The pH profile at a passive current of 1 $\mu A/cm^2$ was found to agree reasonably well with the experimental data of Alavi and Cottis (1985) as seen in Figure 2.7.

Heppner *et al.* (2002) and Heppner and Evitts (2004) developed computational models for the initiation of crevice corrosion. These models calculate chemical

equilibrium, and mass transport to simulate an initiation period in the passive metals. Furthermore, they also modeled the pH profile of a type 304 stainless steel crevice similar to the Alavi and Cottis (1987) experiment. From their result, low pH was observed close to the crevice mouth, and the pH values gradually increased further down the crevice due to crevice expansion. This was in close agreement with experimental observation of most acidic pH values near the crevice mouth and least acidic farther into the crevice.

White *et al*. (2000) predicted a pH of 2.1 near the crevice mouth showing a similar trend to the experimental data of Alavi and Cottis (1987) who obtained a pH of 3 to 4 near the crevice mouth. Their simulation was used to examine the initiation period for bulk solutions of near neutral pH using the critical crevice solution theory.

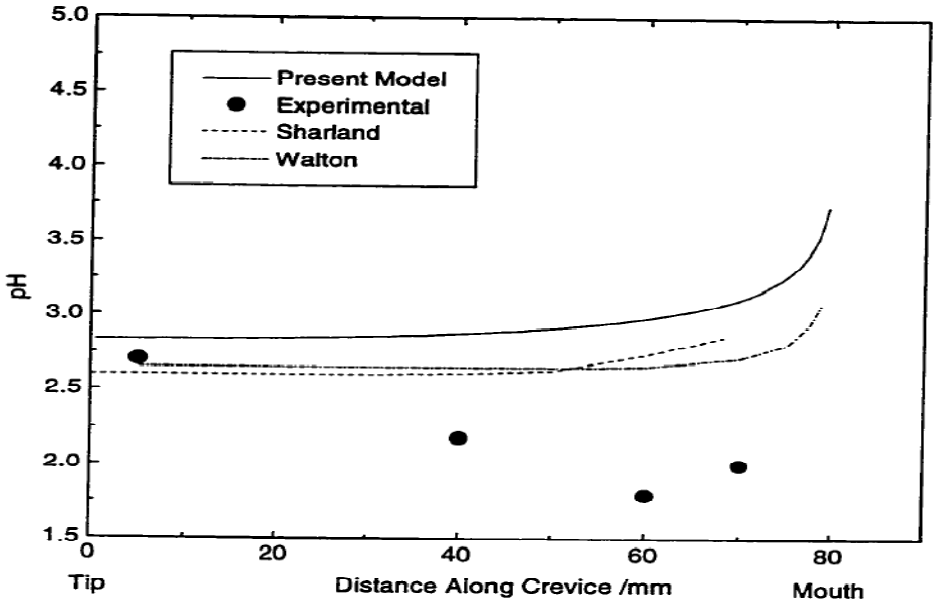

Figure 2.7 Simulation of pH profile in AISI 304 stainless steel crevice corrosion and other modelled results of the Alavi and Cottis Experiment. Passive current density was 1 $\mu A/cm^2$ (reproduced from Evitts *et al.* 1996).

Kennell *et al.* (2008) developed a mathematical model that combined the IR drop and Critical Crevice Solution theories to predict the dynamic crevice pH profile of the crevice of Alavi and Cottis experiment (1987). Figure 2.8 shows the validation of their model and five leading crevice corrosion models against the data of Alavi and Cottis (1987). Their model did predict the most acidic pH values at approximately 1cm from the crevice mouth, whilst the least acidic where found further down the crevice towards the tip. This is in agreement with the dynamic pH behaviour found in the experiment of Alavi and Cottis (1987). Their model was seen as an improvement over other existing models. From their result, they derived three new phases of crevice corrosion namely the total corrosion phase, the dynamic phase, and the quasi-steady state phase.

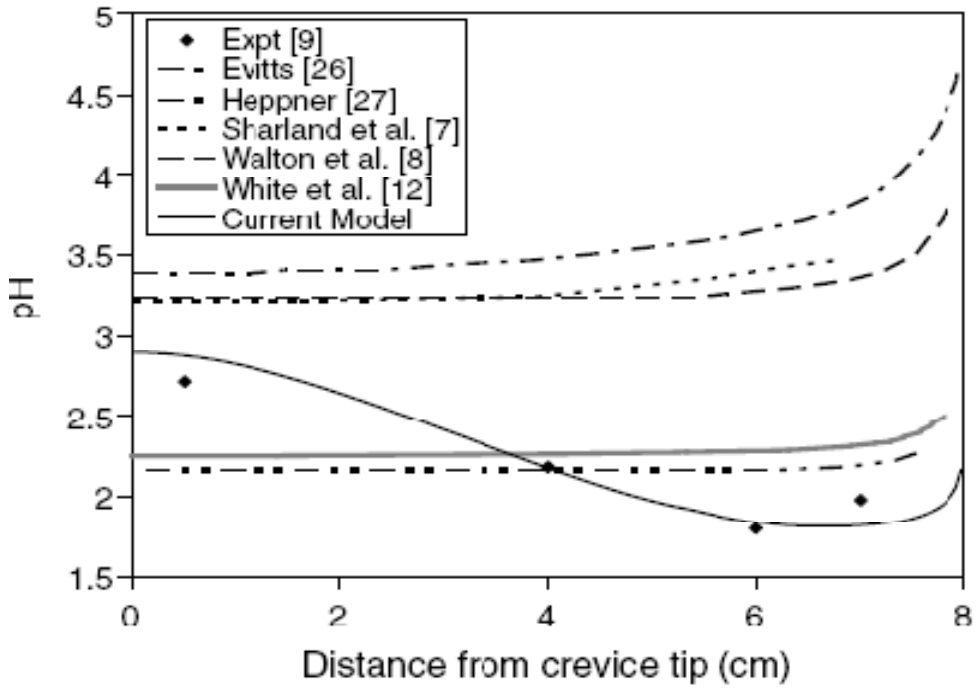

Figure 2.8 Comparison of published models and experimental data for pH profile in a corroding AISI 304 stainless steel crevice (reproduced from Kennel *et al*. 2008).

Furthermore, Kennell *et al.* 2009 numerically modelled the possible cathodic reactions that occur during the crevice corrosion of stainless steel by analysing both the forward and reverse electrochemical reaction, with and without consideration of the hydrogen evolution reaction, HER, that may occur in the crevice. The model without HER showed a steeper concentration gradient close to the crevice mouth and predicts the pH profile similar to that obtained by Alavi and Cottis (1987) as seen in Figure 2.8. The model with HER predicted that the evolution of hydrogen at the tip may be responsible for the steady state concentration gradient of hydrogen ions in the experimental data of Alavi and Cottis (1987).

2.6 Electrochemical Techniques

The corrosion of metals occurs primarily by electrochemical processes involving anodic oxidation and simultaneous cathodic reduction of some species, as well as both an ionic and electrical conduction path between the anode and the cathode. The fundamental understanding of these processes has allowed the development of a number of useful electrochemical techniques for the study of the corrosion phenomena. However, it is not within the scope of this work to mention in details the wide range of the electrochemical methods available for studying corrosion. In this section, the primary electrochemical methods used for measuring the corrosion behaviour in the crevice for this work are described in general.

2.6.1 Faraday's Law

From the literature, it is seen how the combination of Faraday's first and second laws of electrolysis summarizes the equivalence between the amounts of chemical change and electrical energy involved in an electrochemical reaction (Walsh, 1991).

From the first law, the mass of a substance, *W*, deposited or liberated during electrolysis is proportional to the quantity of electricity, *Q*, passed:

$$W \propto Q \tag{2.1}$$

From the second law, the molar mass, *M*, of the reacting material is divided by the number of electrons per molecule, *z* (Walsh, 1991):

$$W \propto M/z \tag{2.2}$$

It follows from equations (2.1) and (2.2) that

$$W \propto Q(M/z) \tag{2.3}$$

Where the constant of proportionality is the reciprocal of the Faraday's Constant, given as 96,487 C mol^{-1} i.e.

$$W = \frac{1}{F} \times \frac{QM}{Z} \tag{2.4}$$

The expression in equation (2.4) can be rewritten conveniently as

$$m = \frac{W}{M} = \frac{Q}{zF} \tag{2.5}$$

The factor $\frac{Q}{zF}$ represents the electrical charge involved in an electrochemical reaction. Equation (2.5) summarizes the equivalence between the amounts of chemical change and the amount of electrical energy.

All metallic corrosion reactions are electrochemical in nature, comprising of an anodic and a cathodic reaction. The rates of the anodic and cathodic reactions must be

equivalent, as determined by the total flow of electrons from the anode to the cathode, known as the corrosion current, I_{corr} (Popov, 1995). Under freely corroding conditions the anodic and cathodic currents (not current densities) are equal (but opposite in polarity) and the corrosion potential attains a level at which equality occurs, i.e. both the anodic and cathodic reactions are polarized from their equilibrium values towards the corrosion potential (Frankel, 2002). If the corrosion current (I_{corr}) can be determined, then it is simple to calculate the corrosion (or penetration) rate using Faraday's laws.

From the corrosion current, corrosion rate can be calculated using Faraday's law as below (Bard and Faulkner, 1980):

$$\text{Corrosion rate (mpy)} = \frac{M_w \mathrm{I}_{corr}}{ZFA\rho} \tag{2.6}$$

where *mpy* is meters per year, M_w is the molecular weight of metal (g/mol), I_{corr} is the corrosion current calculated from the experiments, i_{corr} is the corrosion current density in μA/ cm^2, Z is the number of electrons transferred during electrochemical reaction, F is the Faraday constant (96,487 C mol^{-1}), A is the area of the working electrode (cm^2) and ρ is the density of the metal (g/cm^3).

2.6.2 Galvanic corrosion (GC)

The galvanic corrosion test is a non destructive test as it does not require a potential scan from the active to passive region of the test sample as in the case of an anodic polarization scan. This technique measures the galvanic current and potential simultaneously between two electrically connected identical or dissimilar metals immersed in a solution and held at the same potential. The potential of the corroding

sample in the galvanic couple, also known as the working electrode is usually measured with respect to a saturated calomel electrode (SCE).

For a galvanic couple in a chloride containing environment, at open circuit potential, low cathodic currents are observed which shows that the protective film on the metal surface are still stable. However, as the time of exposure increases, there is a shift from the open circuit potential of the metal from the passive region to the active region due to the attack of the protective film by the chloride ions in the solution. This is characterised by corresponding increase in the galvanic current measured between the electrically connected metals due to the breakdown of the protective film on the more electronegative (anodic) metal of the galvanic couple.

In the case where a crevice is formed between the galvanic couple, the concentration of oxygen dissolved in the bulk environment differs from the concentration in the crevice electrolyte. As the time of exposure increases, differential aeration cells are set up within the oxygen depleted crevice. This site, however, becomes anodic and mass transport of chloride ions into the crevice result in the breakdown of the passive film on the metal surface within the crevice. The graphical output of such an experiment is a plot of log current and potential versus time. A typical galvanic corrosion plot is as represented in Figure 2.9.

The increase in galvanic current in either identical or dissimilar metal couple may be as a result of the small anode to cathode area ratio, high chloride ion concentration, the concentration of oxygen dissolved in the electrolyte and other factors that influence the rate of galvanic corrosion.

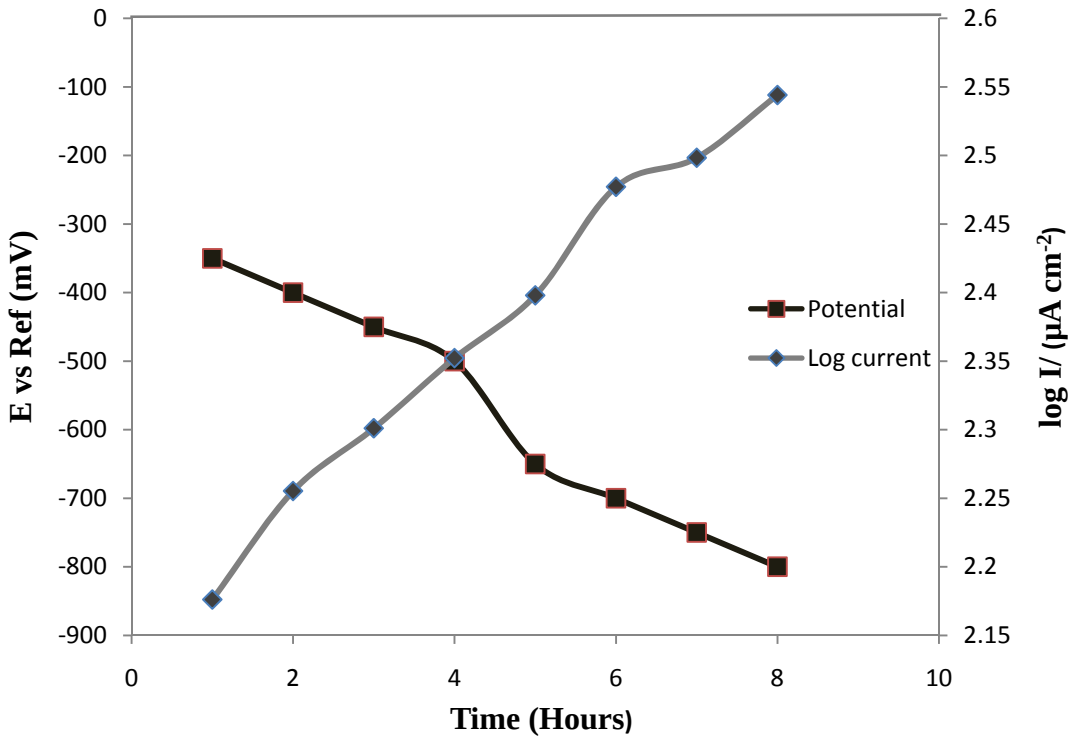

Figure 2.9 A typical galvanic log current-potential curve in 0.5 M NaCl solution.

This technique provides information on the deviation of the open circuit potential as a function of time and the extent of electrical coupling between metals. Creus *et al.* 1997 observed the evolution of the corrosion potential of a titanium/mild steel and aluminum/mild steel galvanic couples in 3 wt % NaCl solution over time. It was observed that the mild steel potential decreased quickly during the first 24 hours of immersion from -460 mV to a steady value of -620 mV in the active region. The potentials of titanium and aluminum increased rapidly as the time of the immersion increased, starting at -420 mV and rising up to -200 mV for titanium after 75 hours, and starting -760 mV up to -730 mV for aluminum.

The galvanic current obtained from the experiment can be used for corrosion rate calculations. A typical galvanic current density, i_g, for an aluminum/steel couple is

300μA cm^{-2} with corrosion rate of 3-5 mm/yr. A titanium/steel couple shows a galvanic current density of 180μA cm^{-2} with corrosion rate of 0.36 mm /yr (Creus *et al.* 1997).

2.6.3 Linear Polarization Resistance (LPR)

The linear polarization resistance scan is a quick and non-destructive technique for measuring the polarization resistance of samples. In this technique, the current response is measured when a small potential sweep is applied to the working electrode. It involves relatively little potential perturbation. A typical potential sweep is usually from -20 mV to +20 mV relative to the open circuit potential of the metal with scan rate of 0.167 mV/s. The scan yields a plot of potential versus current. A linear fit of the plot yields a slope of the applied potential to the measured current *(ΔE/ΔI*), which is the polarization resistance, (R_p), of the sample (Frankel, 2002). The polarization resistance and Tafel slopes, b_a and b_c, can then be used in the Stern-Geary equation to determine the corrosion current and the corrosion rate. The Stern-Geary model equation can be expressed as shown in equation 2.2 (Bard and Faulkner, 1980).

$$R_p = \frac{b_a.b_c}{2.303(b_a+b_c)\times i_{corr}} = \frac{\Delta E}{\Delta I} \tag{2.7}$$

$$R_p = \frac{\Delta E}{\Delta I} \tag{2.8}$$

where R_p is the polarization resistance (ohms), i_{corr} is the corrosion current density (μA/cm^2), b_a and b_c are anodic and cathodic Tafel parameters respectively.

A plot obtained from the LPR technique is as seen in Figure 2.10. The dark blue diamond shapes on the plot are the experimental data generated from the plot and the

black line is the linear fit of the experimental data. From the experimental fit line, the polarization resistance is measured.

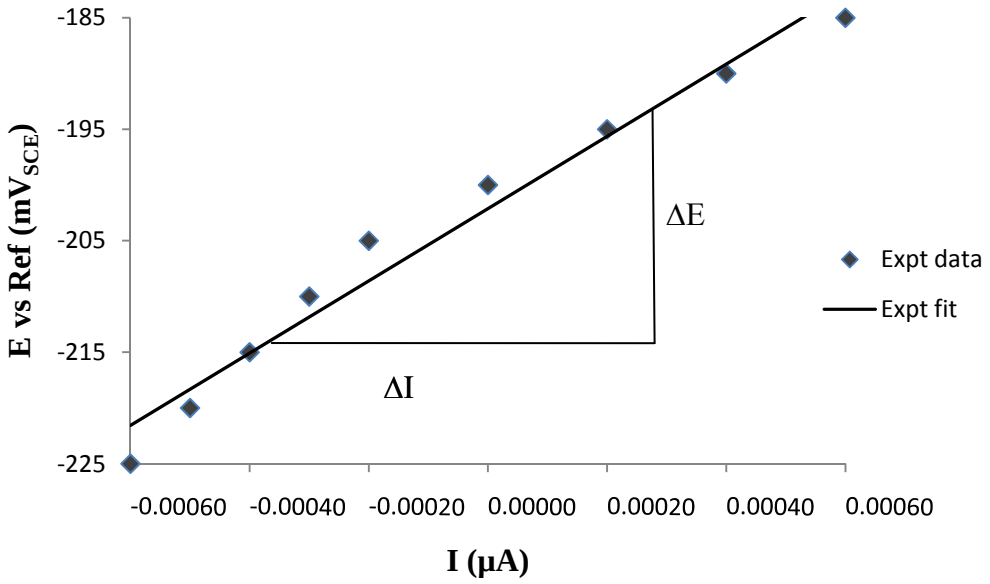

Figure 2.10 A typical potential-current curve obtained from LPR scan.

The major limitation with this technique is that it requires Tafel slopes, b_a and b_c, from the literature or from a potentiodynamic polarization scan to yield a good estimate of the corrosion rate. However, it is suggested that the calculated corrosion rates using Tafel slopes assumed to be 100 mV/decade for b_a and b_c are usually comparable to the corrosion rate calculated from Tafel slopes from potentiodynamic scan by a factor of ±3 mV/dec (Mansfeld, 1976; Scully, 1990; Scully, 2000).

From this technique, the polarization resistance, R_p, measured can also provide information on the corrosion behaviour of the sample studied, where the polarization resistance is inversely proportional to the uniform corrosion rate (Bard and Faulkner, 1980).

2.6.4 Potentiodynamic polarization (PP)

This technique measures the current during a large potential sweep from the cathodic to the anodic region of a sample. It is can be a very destructive test since it involves a large perturbation of the potential from the corrosion potential (Frankel, 2002). The potential of the sample can be ramped from -0.2 V to as high as +1.5 V relative to the open circuit potential, E_{oc}. The technique may use a slow scan rate of about 0.28 mV/s, or a high scan rate of about 16 mV/s. The slower scan rate reveals more details of the corrosion process, such as the passivation area that are not captured during the higher scan rate. Data obtained from the scan are displayed in a plot of potential versus logarithm of the current as shown in Figure 2.11.

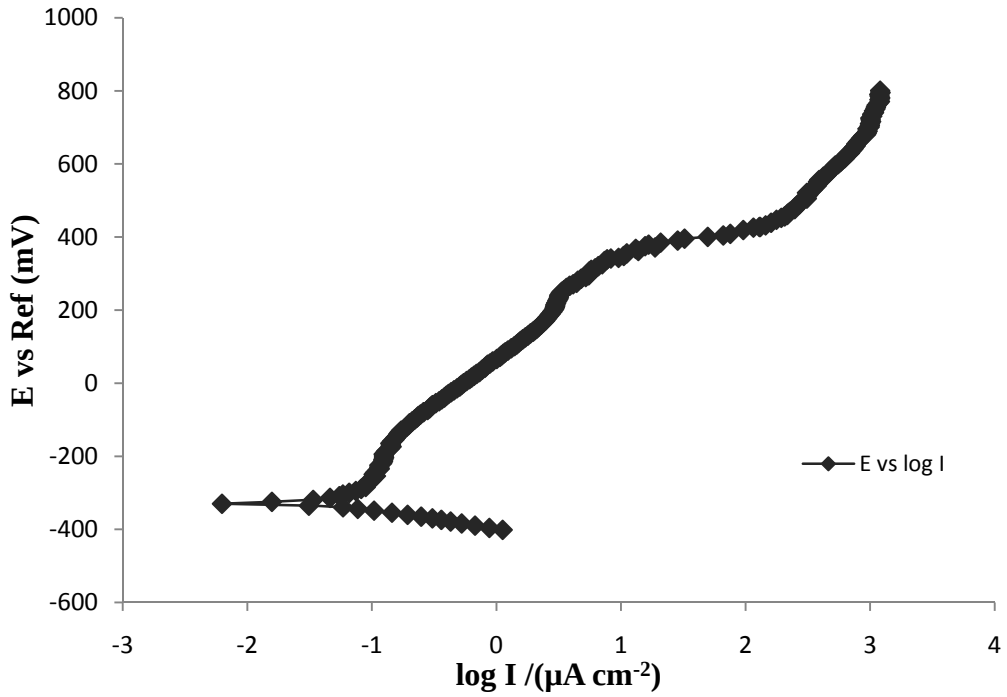

Figure 2.11 A typical potential-log current curve obtained from PP scan.

From the potentiodynamic polarization scan, the Tafel slope, b_a and b_c, for the anodic and cathodic reactions occurring at open circuit may be obtained from the linear extrapolation of the anodic and cathodic regions of the polarization curve, as illustrated in Figure 2.12. These slopes are extrapolated to the point where the anodic and cathodic reaction rates are equivalent, known as the corrosion potential, E_{corr}. The current density at E_{corr}, is the corrosion current density, i_{corr}.

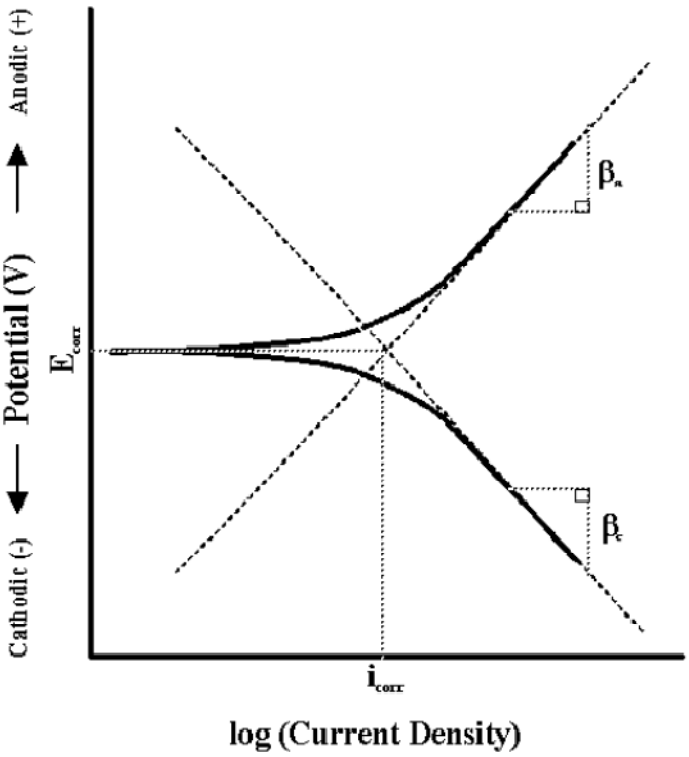

Figure 2.12 Tafel slope calculation (reproduced from Enos and Schribner, 1997).

The Tafel slopes obtained from the extrapolation can be used with the polarization resistance to estimate corrosion rates. Information obtained from the potentiodynamic polarization scan includes, but is not limited to (Popov, 1995):

1. The potential region over which the metal sample remains passive

2. The corrosion rate of the metal in the passive region and the ability of the metal to be spontaneously passivated.
3. The localized corrosion susceptibility of metals.

3 Materials and Methods

This chapter describes the materials and methods used in this study. They are grouped into two sections: the experimental apparatus and the experimental methods. The former section covers the sample preparation, the electrolyte preparation, and the electrochemical measurement equipment used. The latter section describes the various electrochemical methods used for the analysis.

3.1 Experimental Apparatus

3.1.1 Sample Preparation

The engineered crevice was of similar dimensions to the Alavi and Cottis (1987) experimental setup with the absence of pH measuring electrodes. The chemical composition of the AISI 304 stainless steel (AISI 304 SS) sheets and rod used is as listed in Table 3.1. An AISI 304 SS 5 mm thick sheet was machined to produce two rectangular plates with dimensions of 80 mm x 25 mm in the mechanical shop. AISI 304 SS, obtained as a 6.5 mm diameter rod, was cut and machined into four 60 mm long cylindrical working electrodes. The samples were not subjected to any special treatment such as heat treatment, hot or cold working, or passivation treatment. One of the rectangular plates was used as the bottom half of the crevice, the four working electrode

rods were used as the top half of the crevice and the other rectangular plate was used as the bold surface.

The density, ρ, of the metal sample was 7.87 gm/cm^3 with an equivalent weight, E_w, of 25.24 g/equivalent. Copper wire of 30 cm length was soldered to the flat end on top of each four cylindrical working electrodes for electrical connection to the multiplexer. The rectangular plate to be used as the crevice back was placed in a silicone mould and a fast curing epoxy was poured into the mould over the sample. The four cylindrical working electrodes were also immersed in a second mould containing freshly prepared epoxy and positioned at 1 cm, 2 cm, 4 cm and 6 cm from a position defined as the crevice mouth, in a straight line perpendicular to the surface of the mould. While mounting the samples in epoxy, care was taken to avoid any air-bubble sticking to the specimen, since any air-bubbles present between the edge of the specimen and resin will cause localized effects. After curing, both sample/epoxy blocks were taken out of the mould and polished successively with 240, 320, 400, 600 grit silicon carbide papers and finally with up to 0.3 micron diamond paste finish to expose and flatten the surface of the embedded metal samples. This was done in accordance to ASTM G 78 for multiple crevice assembly preparation.

Table 3.1 Chemical composition of type 304 stainless steel (ASM Specialty Handbook: stainless steels), 1994.

Element	C	Mn	Si	P	S	Cr	Mo	Ni	N	Fe
% Value	0.08	2.0	0.75	0.045	0.030	18 - 20	-	8 - 10	0.10	Bal

A polishing jig was locally designed in the mechanical shop for holding the samples in place while carefully polishing, to obtain a flat surface to ensure uniform crevice gap. The second rectangular 304 SS plate was spot welded to a part of the rectangular plate in the crevice back to act as the bold surface for cathodic reactions to simulate an actual crevice corrosion situation. All samples were prepared carefully, and the soldered spots were sprayed with oil based paint to prevent the initiation of corrosion from that part of the sample. After polishing, the specimens were degreased with acetone, cleaned by RO water and dried in hot air. The samples were prepared and kept in a desiccator until one hour prior to the time for the analysis. Immediately before each electrochemical monitoring, the test surfaces were again wet polished with a 0.3 micron finish using diamond paste.

The polished four working electrodes/epoxy block and the rectangular plate/epoxy block were coupled together while submersed in the test solution for each experiment to make sure that there was test solution in the crevice from the onset of the immersion test. The coupling while submersed also helped to eliminate air bubbles in the crevice. Verowhite plastic spacers, described below were used in the assembly, to create varying crevice gaps for each experiment. A crevice gap is the space between the two metal surfaces that are coupled to form a crevice. The coupled crevice assembly was placed in a rectangular channel Plexiglas holder and secured with plastic bolts

using a torque of 5.7 N-m. The individual anode area was 0.31 cm^2 and the total crevice area was 20 cm^2. The test solutions used and their preparation are discussed in section 3.1.2.

The crevice spacers, with thicknesses ranging from 100 μm to 600 μm, were prepared from Verowhite plastic by an Eden V500 rapid prototyper machine. The 100 μm crevice spacer was used to approximate the work of Alavi and Cottis (1987) who used an approximately 90 μm crevice gap in their study. The crevice assembly, not to scale, is shown in Figure 3.1, and the exploded view of the components of the crevice assembly is shown in Figure 3.2.

3.1.2 Electrolyte Preparation

The test solutions used for the experiments were 2 litres of 0.5 M NaCl at a pH of 6.5 and 2 litres of 1M NaCl at a pH of 6. They were prepared using ACS sodium chloride salt and RO water. The test solutions were naturally aerated for at least 15 minutes prior to the *in situ* assembly of the crevice and throughout the experiment. The 4 M KCl solution used as the electrolyte in the four saturated calomel electrodes was prepared using ACS potassium chloride salt and RO water. All experiments were done at room temperature (23 ± 1 °C) and atmospheric pressure (~1 atm).

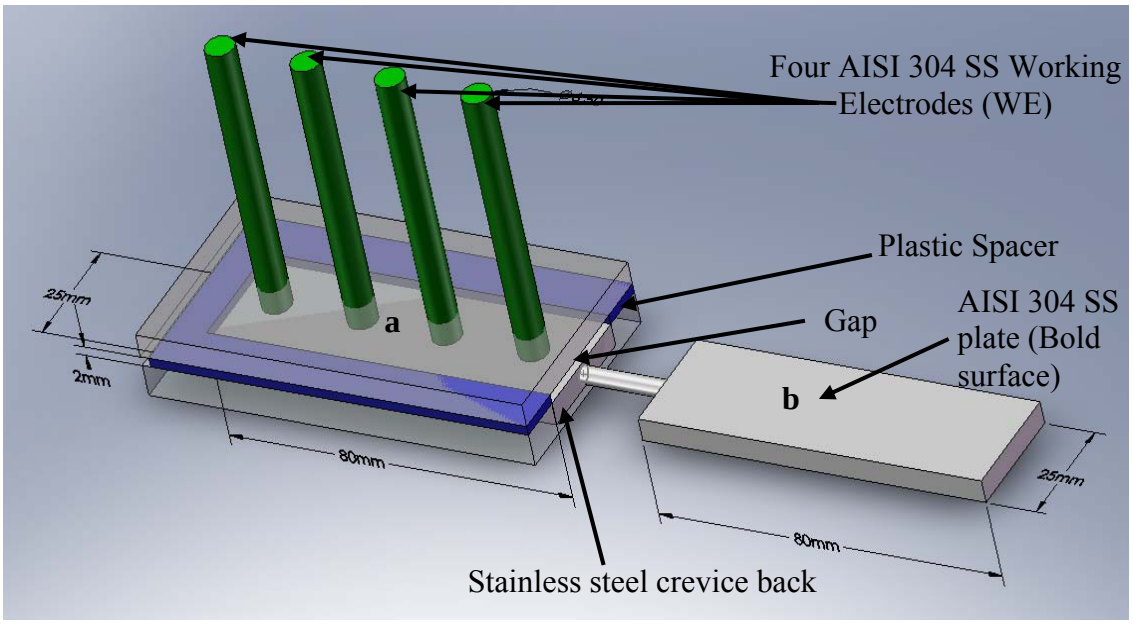

Figure 3.1 The crevice assembly showing an unrealistic crevice gap for illustrative purposes. (a) The anode comprises of four AISI 304 SS working electrodes embedded in epoxy as one part of the crevice, and a rectangular AISI 304 SS plate embedded in epoxy as the other half of the crevice. (b) The cathode (bold surface) is a rectangular AISI 304 SS of same dimensions with the plate in the crevice soldered to a part of the rectangular plate in the crevice back.

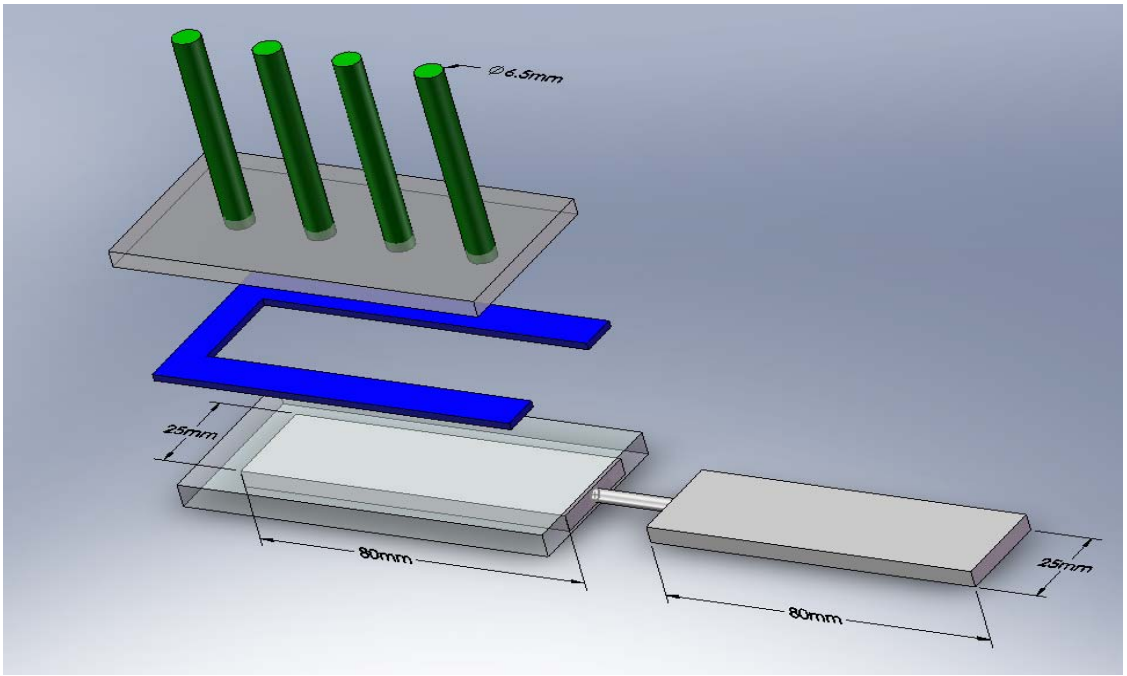

Figure 3.2 The exploded view of the crevice assembly of AISI 304 stainless steel.

3.1.3 Electrochemical Corrosion Measurement Equipment

The electrochemical instruments used were the Gamry PC4^{TM} potentiostat instrument and the ECM8^{TM} Electrochemical Multiplexer as seen in Figure 3.3. The schematic of the crevice assembly as connected to the electrochemical multiplexer is shown in Figure 3.4. Copper wires were soldered to each working electrode in the crevice assembly, to electrically connect the assembly to the Gamry, which was set to the in-line zero resistance ammeter mode. The four active output cables on the multiplexer enabled readings to be taken for the four different electrodes consecutively. The experimental results were displayed on the computer screen and recorded to a data output file. The PC^4 potentiostat was calibrated with the dummy cell for accurate results before the commencement of the LPR test. A 2 litre plastic tank was used for the experiments to ensure complete immersion of the crevice assembly.

a b

Figure 3.3 Photograph of the electrochemical measurement equipments (a) Gamry PC4^{TM} potentiostat (b) ECM8^{TM} Electrochemical Multiplexer.

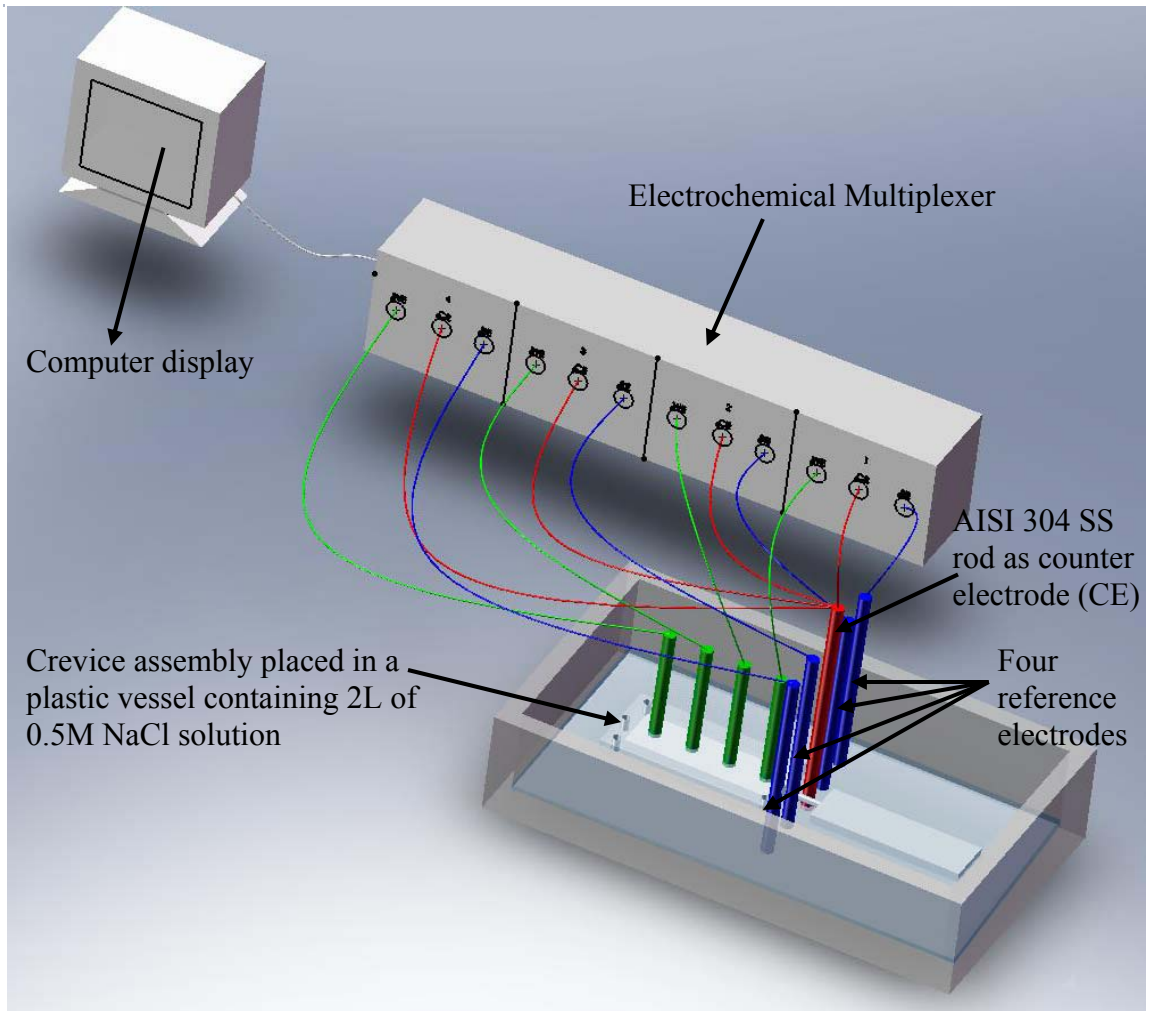

Figure 3.4 Schematic of experimental setup showing the wire connection between the multiplexer and the crevice assembly.

Four saturated calomel electrodes served as the reference electrodes, because the Gamry could not compensate for the IR drop in the crevice when using just a single reference electrode. The counter electrode was a single AISI 304 stainless steel rod and was positioned approximately 2 cm from the crevice opening. The counter electrode material was the same as the metal being studied to avoid contamination of the creviced system with the use of a different material. The sides and the bottom of the crevice were sealed with water-resistant duck tape. The opening was only at the mouth of the crevice

ensuring that the crevice solution was quiescent, i.e. not undergoing significant convective movement of dissolved species in and out of the crevice from the bulk solution.

3.2 Experimental Methods

The following electrochemical analyses, in the sequence of multiplexed galvanic corrosion (MGC), linear polarization resistance (LPR), and multiplexed potentiodynamic polarization (MPP), were carried out to study the onset of crevice corrosion for various crevice gap openings.

3.2.1 Multiplexed Galvanic Corrosion (MGC)

In the MGC method, the galvanic current and potential of the immersed crevice assembly with crevice width of 100 μm to 600 μm, were monitored under free corrosion conditions for a week in a 0.5 M NaCl solution. This was done using the Gamry ECM8 instrument in the multiplexed mode for the 4 locations along the crevice length of the galvanic couple. The multiplexer operates in a multi-channel switch mode where each test channel must be selected prior to commencement of the experiment. The sampling time of 0.166 hours and total test duration of 168 hours were accurately added to the setup dialog box prior to the commencement of MGC measurement.

The total cathode area to anode area ratio was 2.5:1. The temperature of the test electrolyte was 23 ± 1˚C. After the one week testing period elapsed, the crevice assembly was removed from the test solution. The creviced part was opened, washed

with RO water, and dried for inspection of each location along the crevice under the optical microscope. Information on the corrosion current, $I_{corr,}$ and the corrosion current density, i_{corr}, over the exposed area of the working electrode, $A,$ was obtained from the galvanic corrosion output file of the Gamry multiplexer. A similar test was done for a crevice width of 100 μm in a 1 M NaCl solution to compare crevice corrosion initiation in the more concentrated electrolyte. Results obtained will be discussed in Chapter 4.

3.2.2 Linear Polarization Resistance (LPR)

For the LPR method, the crevice assembly was left in the 0.5 M NaCl solution for 24 hours to obtain stable passive film conditions. The metal in the crevice was then polarized to ±20 mV around the open circuit potential (E_{corr}) with a scan rate of 0.125 mV/sec and a sample period of 2 seconds while measuring the total resistance of the solution at each location along the crevice. The polarization resistance, R_p, and the corrosion current, I_{corr} was obtained from the log current versus potential plot. This test was not done in the multiplexed mode because the Gamry multiplexer was not designed with provision for a multiplexed LPR mode. Results obtained from this technique will be discussed in Chapter 4.

3.2.3 Multiplexed Potentiodynamic Polarization (MPP)

The MPP method required polarizing the sample over a wide range of potential sweep, from -0.2 V in the cathodic region, to +1.2 V in the anodic region, in order to examine the overall corrosion behaviour along the crevice length in the multiplexed mode. The test was done with a scan rate of 3 mV/s and a sample period of 1 second.

However, since this test is destructive, it is expected that the high dissolution rate of the sample at all four positions in the crevice will cause severe changes in the crevice solution. These changes in the crevice electrolyte composition may alter the metal surface, thereby affecting the region of passivity of each position along the crevice. In effect, such alteration during the experiment may not yield useful information. Preliminary results obtained from this technique will be discussed in Chapter 4.

The detailed description of the materials and the methods used for the corrosion measurement of an AISI 304 SS crevice coupled to AISI 304 SS bold surface at various electrolyte concentration and crevice width was covered in this chapter. In the next chapter, the experimental challenges encountered during this research, and the proposed corrective measures are discussed. In addition, the galvanic corrosion rates obtained from the MGC experiment for various locations along a crevice of AISI 304 SS metal, and its comparison with the measured polarization resistance, R_p, from LPR experiment are discussed.

4 Results and Discussion

This chapter presents the discussion on the current and potential variations, and the estimated corrosion rate at different positions along the AISI 304 SS crevice obtained from MGC, LPR, and MPP measurement techniques. The crevice corrosion rates calculated for all four positions along the crevice from the galvanic corrosion (MGC) test, were compared with the polarization resistance (R_p) values measured at the similar positions along the crevice.

To assess the effectiveness of these techniques in providing information on the corrosion behaviour at different positions along the crevice, preliminary tests were done with different samples. The test electrolytes used were 0.5 M and 1 M NaCl solutions, with varying crevice widths of 100 μm to 600 μm at room temperature. The results obtained from the MGC test using 0.5 M NaCl solution will attempt to reproduce a peak current behaviour at the position closest to the mouth of an AISI 304 SS crevice. This is to validate the peak pH value observed at similar position in the work of Alavi and Cottis (1987) and the model prediction of Kennell *et al.* 2009. Table 4.1 summarizes the test conditions and the results obtained along the crevice for each sample studied.

From the preliminary results, the MGC tests showed good results with high anodic current behaviour at 1 cm from the crevice mouth and low cathodic currents at 2 cm, 4 cm and 6 cm from the crevice mouth for Samples A to G, with the exception of

sample D that showed high anodic current at 6 cm. The results obtained from the LPR and MPP measurement carried out on samples with 100 μm crevice width did not yield good results due to concentration gradients in the crevice, and as such the results were discarded.

Table 4.1 Summary of the electrochemical measurements of crevice corrosion in AISI 304 stainless steel.

Crevice Width	Crevice Assembly	NaCl Solution Concentration	Type of Test	Duration of Test
100 μm	A	0.5 M	MGC	24 hours
100 μm	B to G	0.5 M	MGC	168 hours
200 μm to 600 μm	1 to 5	0.5 M	MGC	24 hours
100 μm	C and D	0.5 M	LPR and MPP	2 seconds
100 μm	H and I	1 M	MGC	168 hours

The MGC tests carried out on Samples 1 to 5 with 200 μm to 600 μm crevice widths did not yield good results and were discarded, where initiation of crevice corrosion did not occur, due to the large crevice widths. The LPR and MPP tests were not done with the crevice widths ≥ 200 μm due to experimental uncertainties associated with larger crevice widths.

In summary, the results obtained from the MGC tests with 100 μm crevice widths shows that corrosion will initiate at approximately 1 cm from the crevice mouth.

All the experimental challenges encountered in this work and the proposed corrective measures will be presented in section 4.1.

4.1 Experimental Challenges

Crevice geometry is a very critical factor in the crevice corrosion process. Crevice width and depth control oxygen access into localized areas, and thereby influence the concentration gradient and potential distribution within these areas. The difficulties associated with ensuring reproducible and repeatable crevice geometries and even metal surface for this work are as discussed below.

During the sample preparation, hand polishing of the crevice components caused physical irregularities along the crevice length such as surface unevenness of the metal/epoxy parts in the crevice. These variations affected the observed current and potential behaviour in the crevice. Such irregularities resulting from uneven pressure applied to the crevice test samples during hand polishing, caused the crevice gap to be wider than desired, which can increase the IR drop along the crevice and decrease the anodic current, depending on the degree of unevenness (Agarwal, 2007). Therefore, to address the problem of surface unevenness, a polishing jig was locally designed to mechanically hold the crevice sample parts in order to achieve an even surface finish while polishing up to the 0.3 micron finish with diamond paste.

Furthermore, to achieve a reproducible crevice width for all experiments, a torque wrench was used to secure the plastic bolts of the crevice assembly. However, for a crevice designed with metal samples embedded in an epoxy resin, as used for this study, the torque application consistency was very difficult to maintain to achieve

constant and reproducible crevice geometries during each test. The variation in the tightness of the crevice assemblies for each experiment caused the current and potential behaviour observed along the crevice to vary with poor reproducibility. The temperature of the test environment had no influence on the tightness of the crevice.

For cases where assembling of the crevice resulted in wide crevice gaps, the crevice did not undergo crevice corrosion and it was assumed that the crevice electrolyte assumed the bulk electrolyte concentration. Also, in cases where the plastic bolts for the crevice assembly wore out, and the torque applied caused the bolts to be screwed too tight, the test electrolyte was not able to penetrate into the crevice, and this resulted in the absence of crevice corrosion. The absence of crevice corrosion was due to the tightness of the crevice geometry, which causes mass transfer limitations of ionic species in and out of the crevice. The tightness of the coupled crevice assembly could not be inspected using the optical microscope before and after each experiment because of the structure of the assembly.

It was found that re-polishing and re-using a sample did not yield reproducible results. It was assumed that the re-polishing of the already used samples was not sufficient to create metal surface free of the pits that developed from the previous long hours of exposure in the test electrolyte. The presence of such surface imperfections on the metal surface can cause higher corrosion current to be observed at the locations that were affected by those pits than with a newer sample.

Another area of concern was the polymer used to create the artificial crevice gaps. The spacers used for the experiment were made of Verowhite plastic, and can shrink when compressed for long duration. The severity of the shrinking could not be

determined, since the spacers were designed with a thickness in the order of microns. Therefore, new plastic crevice spacers were used for each set of experiments, to ensure consistency in the crevice gap created for each test. In summary, to achieve the aim and objective of this work, sample preparation with the appropriate instruments and consistent environmental conditions is of great importance, to control the variability of the laboratory data with field data.

4.2 Room Temperature Experiments

4.2.1 Galvanic Current and Potential in 0.5 M NaCl solution

To study the effect of an increase in crevice width on the initiation time for crevice corrosion of the AISI 304 SS galvanic couple, galvanic corrosion test were carried out using crevice gaps ranging from 100 μm to 600 μm. From the results obtained with 24 hours exposure for all crevice widths, high corrosion current was observed for the location that was 1 cm from the crevice mouth for the 100 μm crevice width. However, low cathodic current was recorded at all four positions along the crevices with widths of 200 μm, 300 μm, 400 μm, 500 μm and 600 μm. In the latter cases, there was no initiation of active crevice corrosion, and such a delay in crevice corrosion initiation is typical of wider gaps, due to the fact that the crevice electrolyte assumes the bulk electrolyte concentration, and therefore a longer time is needed for the pH within the crevice to drop low enough to cause the breakdown of the protective film.

This is in close agreement with the prediction of Alavi and Cottis (1987), that a wider crevice gap reduces the chloride ion activity in the crevice of AISI 304 stainless

steel, thereby increasing the corrosion initiation time. On that note, the test using crevice widths of 200 µm to 600 µm was discontinued, with emphasis placed only on the 100 µm crevice width. For the galvanic current and potential behavior of an AISI 304 SS crevice with 100 µm crevice width, different Samples A to G were studied. Samples A to D were prepared by hand polishing, where as Samples E to G were prepared using the mechanical jig for polishing. The discussion on the current and potential variations observed along the crevice for Samples A, B, C and D are presented in this section. The plots for Samples E to F are found in Appendix C1. The galvanic current behavior observed for Sample A with 100 µm crevice width after 24 hours is as shown in Figure 4.1.

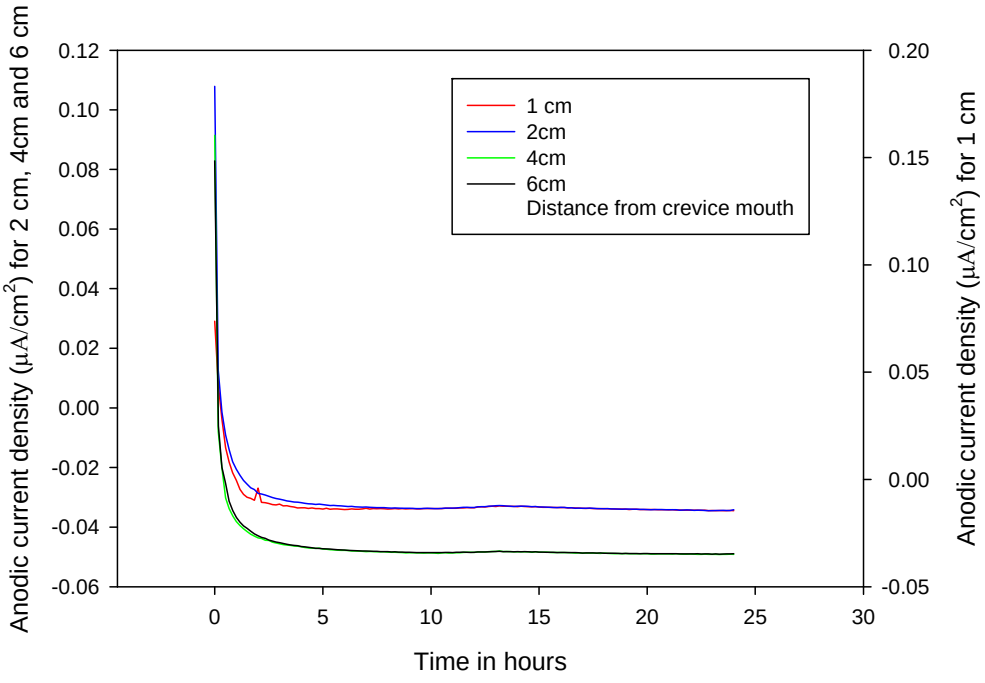

Figure 4.1 Galvanic current plot for AISI 304 SS crevice (Sample A) with 100 µm gap for 24h at pH of 6.5 and room temperature.

From the figure, it can be seen that when the crevice assembly was initially immersed in solution at t < 1 hour, the passive film on the metal surface at each location

in the crevice became destabilized, which is observed with anodic current density up to 0.1 μA/cm^2. However, the anodic current quickly declined within the 1 hour to low cathodic current values for 1cm and 2 cm from the crevice mouth, and stayed low throughout the 24 hours exposure time. The current at 4 cm and 6 cm was at open circuit throughout the experiment, this may be probably due to loose connections of the copper wires soldered to the working electrodes to the Gamry.

The observed decrease in the current density at 1 cm and 2 cm at t < 1 hour shows that the passive film on the metal surface in the crevice re-stabilized after few minutes of immersion, and remained in the incubation stage during the 24 hours exposure period. Similar repassivation behaviour of passive alloys has been reported by few researchers (Evitts, 1997; Jones and Green, 1969). These authors report that when passive alloys are initially immersed into a solution, the passive current density rapidly increases to values that may be larger than 10 μA/cm^2, and then, within 1 hour, decline to approximately 1 μA/cm^2.

The 24 hours experiment indicated that accelerated dissolution of the metal surface will occur as a result of oxygen depletion in the crevice, and high chloride concentration and low pH in the crevice (Shi, 1990). Griess (1986) also showed that the magnitude of the active / passive current density during crevice corrosion of titanium is very dependent on the solution pH inside the crevice and temperature. Therefore, to establish the onset of crevice corrosion for an AISI 304 SS crevice, the duration of the galvanic corrosion test was increased to one week. This was to allow conditions to develop in the crevice the way it is in service environments.

For the long term exposure, a second crevice, Sample B with crevice width of 100 μm was assembled, and immersed in a 0.5 M NaCl solution for one week to observe the current and potential behaviour. Similar to previous experiment, at the onset of the experiment, high anodic current of about 5 $\mu A/cm^2$ and 0.04 $\mu A/cm^2$ was observed for the 1 cm and 2 cm position from the crevice mouth at $t < 1$ hour. Within 1 hour of exposure, the current densities decreased to a current density of approximately 2 $\mu A/cm^2$ for 1 cm from the crevice mouth and a cathodic current density of -0.03 $\mu A/cm^2$ for 2 cm from the crevice mouth.

During the one week exposure, high anodic current was observed at 1 cm from the crevice mouth. The current density gradually increased from 2.5$\mu A/cm^2$ at 24 hours up to 6.8 $\mu A/cm^2$ after 168 hours. However, very low and steady cathodic currents were observed at 2 cm, 4 cm and 6 cm from the crevice mouth throughout the experiment as seen in Figure 4.2. The sharp spike in current observed at 167^{th} hour for the location 2 cm, maybe due to initiation of pits at the site.

According to the CCST and IR drop theories, it is expected that during the onset of crevice corrosion, 1cm from the crevice mouth will experience less IR drop effect with the bold surface and thus acts like the anodic site (Pickering, 1993; Kennell *et al.* 2008; Bocher *et al.* 2008).

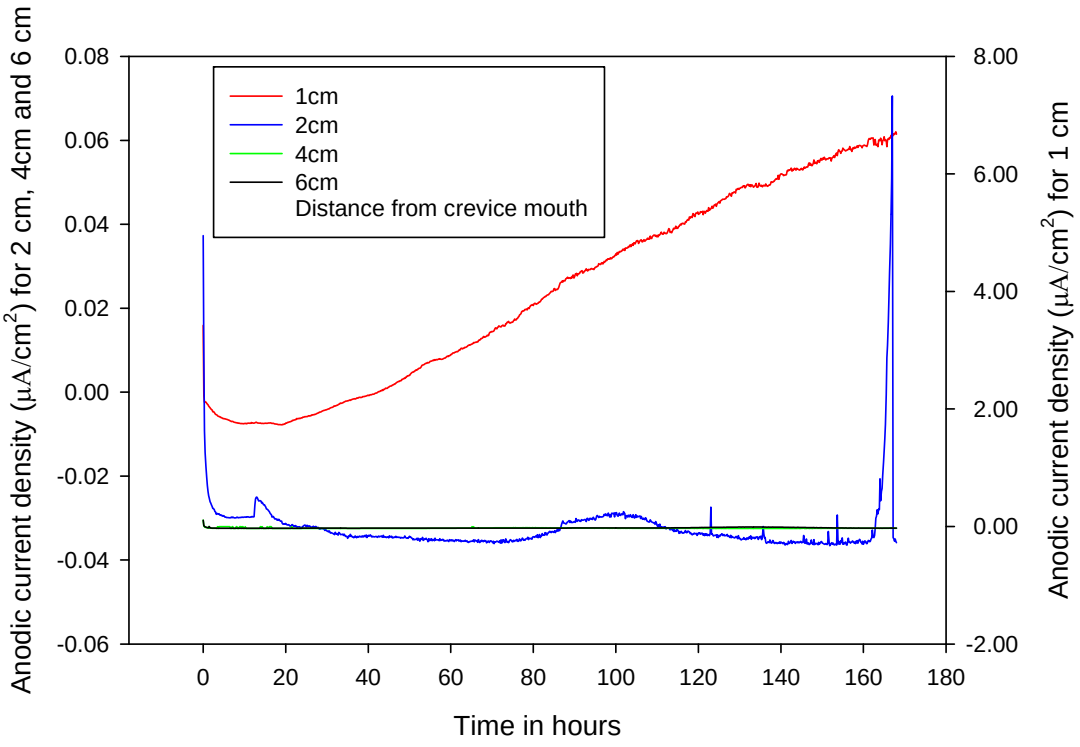

Figure 4.2 Galvanic current behaviour along AISI 304 SS crevice (Sample B) with 100 μm gap for 168h at pH of 6.5 and room temperature.

From the figure above, it is seen that during the incubation period of 24 hours, mass transport of ionic species which occurs between the bulk and crevice solution causes metal dissolution within the deoxygenated crevice. The hydrolysis of the metal ions causes a gradual pH decrease in the crevice. Furthermore, an increase in the influx of anions such as chloride ions from the bulk solution into the crevice solution leads to a development of critical crevice solution with low pH and high Cl^- ion concentration (Oldfield and Sutton, 1978). The critical crevice solution leads to the loss of stability of the passive oxide layer in the crevice, and due to the low IR drop between the bold surface and the position closest to the crevice mouth, the cathodic oxygen reaction on the bold surface drives the anodic dissolution at this site (Kennell *et al.* 2008; Kennell *et al.* 2009; Alkire, 1985). The result is the initiation of crevice corrosion as seen by the

increasing anodic current at 1cm from the crevice mouth. The pH and Cl^- ion level in the crevice plays an important role in the initiation of crevice corrosion. It is suggested that the pH inside the crevice decreases during the induction period and crevice corrosion occurs for type 304 stainless steel at pH of 2 (Shi, 1990) and at pH of 1 for Titanum (Mckay and Mitton, 1985).

However, as the distance into the crevice increases, large IR drop is established between the bold surface and these positions in the crevice due to ohmic considerations, and lower anodic dissolution is observed further into the crevice. This may be due to the fact that the locations further down the crevice are under anodic control and thus the solution composition, the pH, and the potential inside the crevice change (Kennell *et al.* 2009; Bocher *et al.* 2008). Furthermore, hydrogen reduction reactions at the bottom of the crevice may lead to an increase in pH with a corresponding drop in the corrosion current at these locations (Hua and Ives, 1998; Alavi and Cottis, 1987). Therefore, the inability of these sites further into the crevice to couple with the cathodic reactions occurring on the bold surface stifles the drive of anodic reaction inside the crevice.

The peak anodic current density observed at 1 cm from the crevice mouth is in close agreement with the experimental results obtained from an AISI 304 SS metal/non-metal crevice by Alavi and Cottis (1987). From their study, they reported a peak pH of 1.7 at approximately 2 cm from the crevice mouth after 20 hours of immersion, and the least acidic pH at locations deeper into the crevice. The low pH value observed in their experiment corresponds to the high corrosion current observed at 1 cm from the crevice mouth in this study. Mathematical models by various researchers also show low pH

values observed at approximately 1 cm from the crevice mouth (Hua, 1998; Kennell et al, 2008; Kennell et al, 2009; Evitts *et al*. 1996; Heppner *et al*. 2002).

Similar behaviour was observed for a repeat experiment with Sample C using 100 µm crevice width as shown in Figure 4.3.

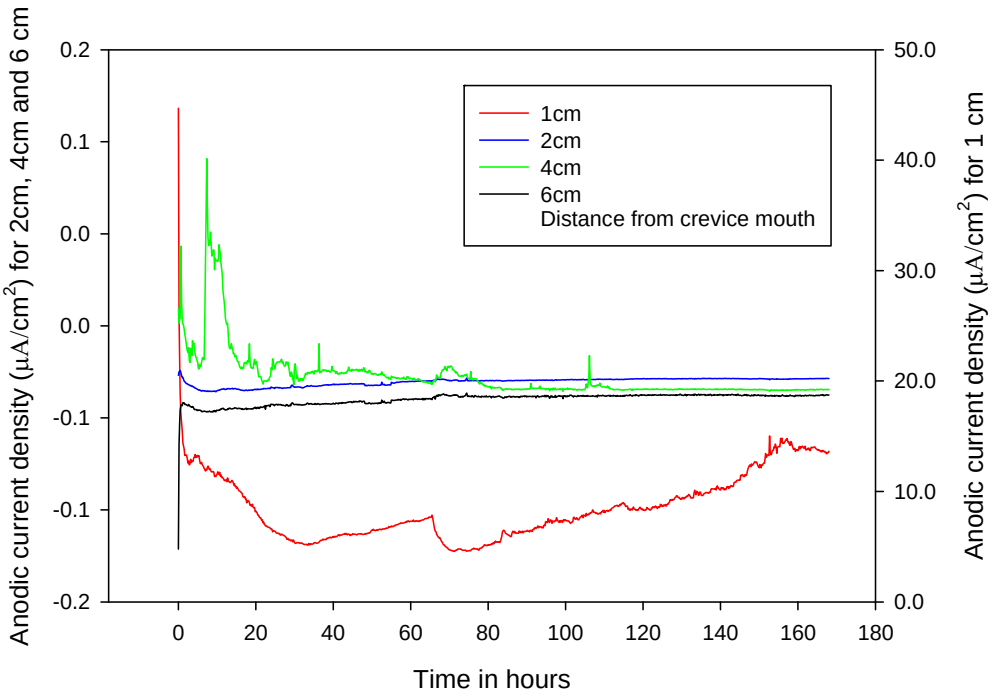

Figure 4.3 Galvanic current behaviour along AISI 304 SS crevice (Sample C) with 100 µm gap for 168h at pH of 6.5 and room temperature.

At the onset of the experiment, high corrosion current was observed at 1 cm from the crevice mouth, and very low cathodic current was observed at 2 cm, 4 cm and 6 cm from the crevice mouth. The large current observed at 1 cm from the crevice mouth shows similar trend of the initial destabilization of passive film on immersion of the crevice assembly. The corrosion current then began to decrease after 0.5 hour, probably due to the ability of the protective oxide film to quickly grow and re-stabilize. After 24 hours, gradual increase in current was observed. The fluctuation in current

observed after 72.5 hours was as a result of the addition of test electrolyte to the system after 3 days to account for evaporation losses of the test solution. The addition of the electrolyte probably dilutes the chloride ion concentration in the crevice electrolyte, which reflects as a sharp decrease in the anodic current. The current, however, stabilizes after an hour and increases as the time of exposure increases.

Contrary to the observed trend, with a high corrosion current observed at 1 cm from the crevice mouth, a fourth repeat test using a 100 µm crevice width in a 0.5 M NaCl solution for 168 hours showed a peak current up to 4.1 µA/cm^2 at 6 cm from the crevice mouth, being the closest to the crevice bottom as seen in Figure 4.4. Very low corrosion current was observed at 1 cm, 2cm and 4 cm from the crevice mouth.

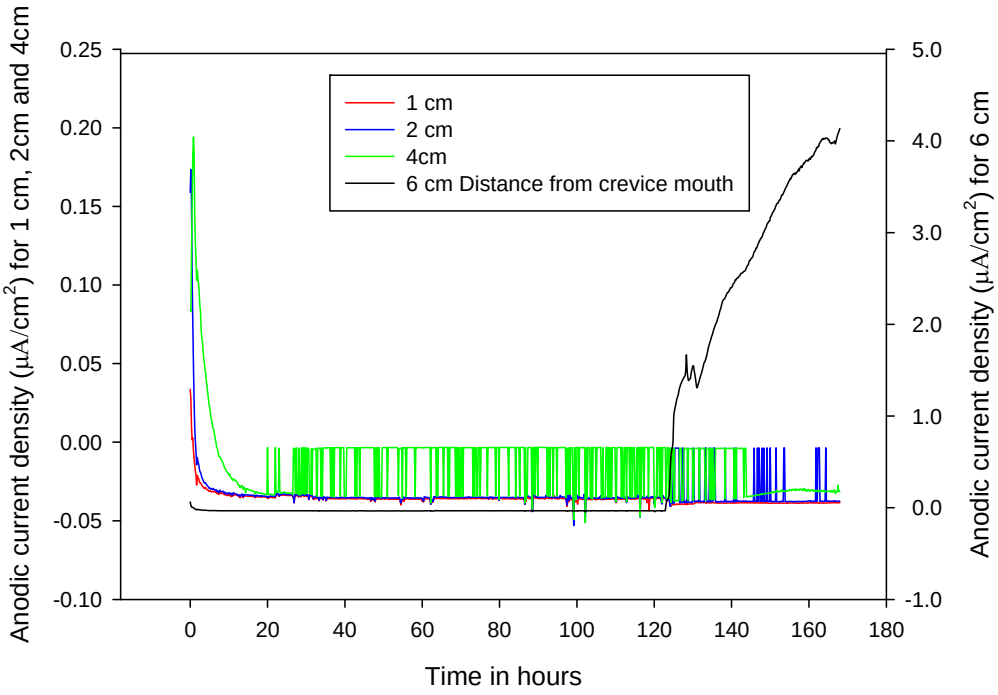

Figure 4.4 Galvanic current behaviour along AISI 304 SS crevice (Sample D) with 100 µm gap for 168h at pH of 6.5 and room temperature.

This deviation from the previously observed large anodic current behaviour at 1 cm from the crevice mouth, and with a peak current at 6 cm from the crevice mouth shows the stochastic nature of crevice corrosion. Factors like surface imperfections, variation in the crevice width and metallurgical inhomogeneities may account for the difference in the initiation site for this experiment. Furthermore, the current noise behaviour observed at 4 cm from the crevice mouth may be due to hydrogen evolution reaction occurring at this site in the crevice. The presence of hydrogen bubbles at this site makes it become cathodic with respect to the bold surface. Similar behaviour at locations close to the crevice tip in an AISI 304 SS crevice was predicted in the model by Kennell *et at.* 2009. From these sets of experiments, it has been established that the largest corrosion current in an AISI 304 SS crevice is observed at 1 cm from the crevice mouth for most samples studied in 0.5 M NaCl solution. Only one sample displayed the stochastic nature of crevice corrosion initiation at 6 cm from the crevice mouth. These current evolution data validates the model predictions of Kennell et al. 2009 and is in close agreement with the pH profile observed by Alavi and Cottis (1987) for AISI 304 SS crevice corrosion.

From the MGC tests carried out, the calculation of the corrosion rates of the galvanic couple of AISI 304 SS crevice in the 0.5 M NaCl solution using the Faraday's law and the galvanic current densities, i_{corr}, obtained from the MGC tests for all crevice width studied are shown in Appendix B. The current densities and the calculated corrosion rates obtained for various galvanic couple of 100 μm crevice width, with the location along the crevice relative to the crevice mouth, which shows the highest corrosion current, are shown in Table 4.2. It is known that the magnitude of the galvanic

current provides an indication to the severity of the corrosion rate that will be observed between a galvanic couple (Baboian, 1976). The calculated corrosion rates of the galvanic couple made of the identical AISI 304 SS are very low as seen in Table 4.2.

Table 4.2 Calculation of the corrosion rates of AISI 304 SS galvanic couple in 0.5 M NaCl solution (crevice width of 100 μm) at room temperature, 6.5 pH and 168 hour of exposure.

Sample tested	Location with highest corrosion current(cm)	I_{corr} (μA)	i_{corr} (A/cm^2)	Corrosion rate (mmpy)
C	1	8.593	2.772×10^{-5}	0.145
D	6	0.6951	2.242×10^{-6}	0.012
E	1	0.3844	1.239×10^{-6}	0.007
F	1	0.5204	1.677×10^{-6}	0.009
G	1	3.705	1.195×10^{-5}	0.063

This low galvanic current is typical of coupling metals with the same reduction potential. The influence of the cathode area size, which was twice the anode area size on the corrosion rate, was negligible. Therefore, it can be inferred that when two AISI 304 SS metals are coupled galvanically under similar conditions, the measured corrosion rate will be low.

Having studied the current behaviour along different positions in the AISI 304 SS crevice, the information on potential variations along the crevice generated from the MGC tests will be discussed to see the relationship between the measured current and the corresponding potential variation along the crevice. The open circuit potential of an

AISI 304 SS galvanic couple immersed in 0.5 M NaCl with varying crevice widths is as shown in Figure 4.5. The open circuit potential is the potential of a freely corroding galvanic couple, and was measured 10 minutes before the start of the MGC test.

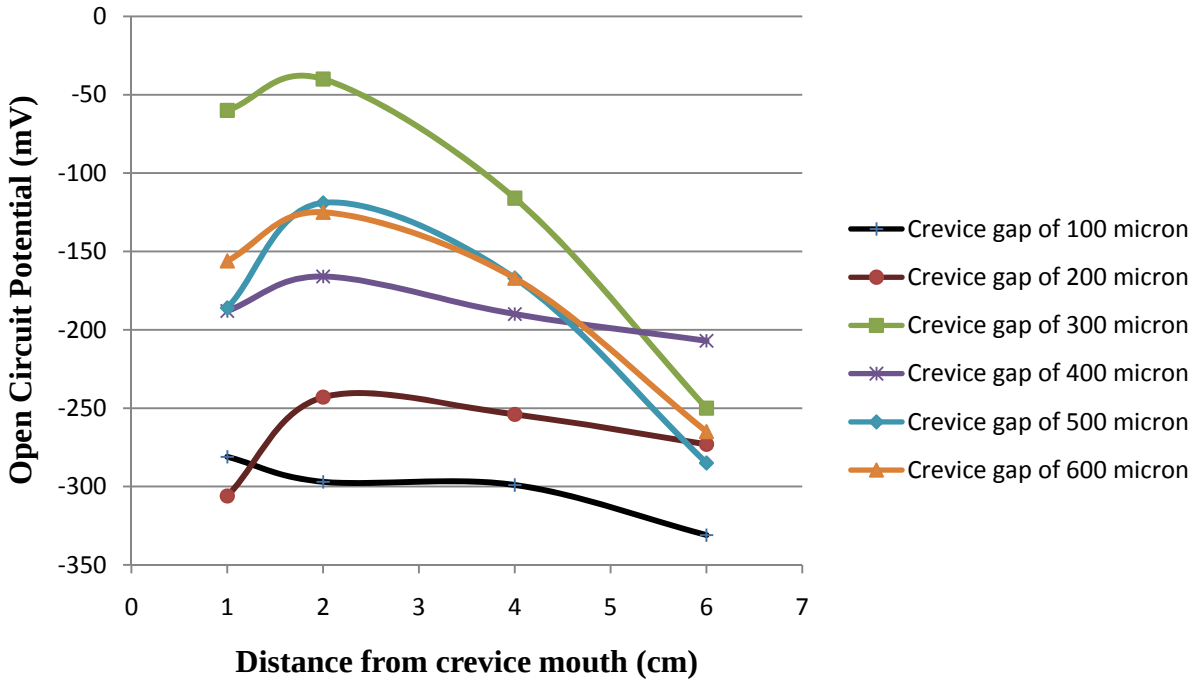

Figure 4.5 Open circuit potential along an AISI 304 SS crevice length for 100 µm to 600 µm crevice widths immersed in 0.5 M NaCl solution.

The trend in Figure 4.5 shows that as the crevice gap becomes wider, the OCP increases to more positive (noble) values, from -350 to -50 mV (SCE). An increase in open circuit potential in the noble direction is seen as the depth is increased from 1 to 2 cm from the crevice mouth. As the depth increases from 2 to 6 cm, the OCP then drops. Furthermore, during the 168 hours of the MGC tests, the potential behaviour at all four locations along the crevice was measured against SCE and recorded for all sample studied. Figure 4.6 shows the variation of potential with distance from the crevice mouth in 168 hours for Sample C.

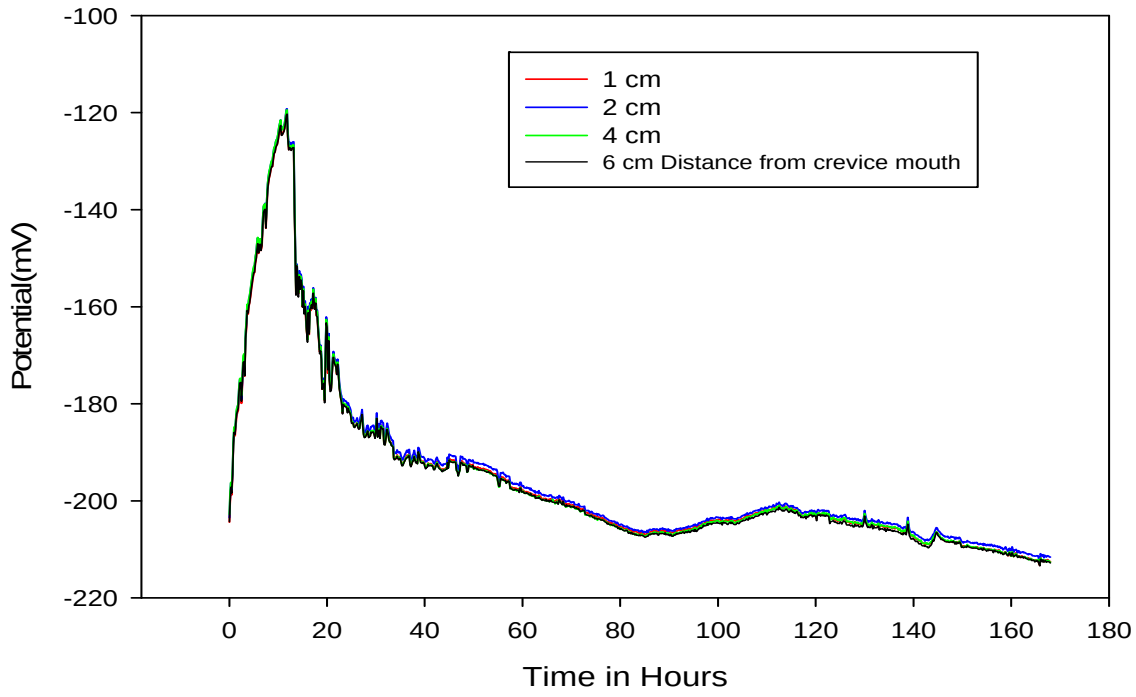

Figure 4.6 Variation of potential with time along the AISI 304 SS crevice with 100 µm gap immersed in 0.5 M NaCl solution for 168h at pH of 6.5 and room temperature.

From the figure, it is seen that at the onset of the experiment, the potential values along the crevice initially increases towards the noble direction, which may be due to the diffusion of oxygen into the crevice electrolyte during this induction period. However, as differential cells are set up and the crevice becomes active, the potential values decrease to active values in the vicinity of the corrosion potential of the sample. This decrease to negative potential values indicates the initiation of crevice corrosion. Therefore, it is assumed that the measure of corrosion initiation is based on the time the anodic current density increases, with a corresponding potential decrease in the crevice (Shi, 1990).

As seen in Figure 4.3 and 4.6, the sudden increase in current with the corresponding decrease in corrosion potential in the crevice was observed after 24

hours. However, as the time of exposure and distance into the crevice increases, the potential values, displays a more steady-state-like behaviour. This variation in potential is identical for all four locations along the crevice, and this may be due to the fact that active corrosion can occur along a crevice without significant change in the corrosion potential of the sample. This behaviour is similar to that reported by Griess (1968) during the crevice corrosion of titanium alloys in aqueous salt solutions. From the observed trend, it is assumed that the potential change in the crevice is independent of the location in the crevice regardless of the local current. Therefore, increase in anodic current density at each location in the crevice will slightly shift the potential to values just below the corrosion potential of an AISI 304 stainless steel.

Having looked at the current and potential variations in the crevice using the 100 μm in the 0.5 M NaCl solution, further studies were carried out using the 1 M NaCl solution on Sample H and I to study the effect of increase in electrolyte concentration on the initiation of crevice corrosion during one week exposure.

4.2.2 Galvanic Current and Potential in 1 M NaCl solution

For the samples with crevice width of 100 μm immersed in a 0.5 M NaCl solution, it was observed that the incubation period lasted 24 hours, and then the current began to rapidly increase as seen in Figure 4.2 and 4.3. However, the experiment carried out using Samples H and I with a crevice width of 100 μm immersed in a 1 M NaCl solution did not show any increase in current after 24 hours, and all through the one week exposure time. Furthermore, at the end of each experiment, physical examination

of the metal surface on the crevice showed no evidence of detectable localized attack on the samples.

It is assumed that an increase in the chloride concentration of the bulk solution to 1 M will raise the chloride level of the crevice electrolyte. This increase in chloride level in the crevice may cause rapid breakdown of the protective passive film formed on the metal surface, resulting in nearly immediate crevice corrosion initiation as compared to the case of the 0.5 M systems having an incubation time of approximately 24 hours. This observed delay in corrosion initiation may also be due to experimental inconsistencies such as variations in surface evenness, resulting in a wider crevice width compared to very tight crevices that cause severe crevice corrosion of austenitic stainless steels (Alavi and Cottis, 1987). The experiments using 100 μm crevice widths in 1 M NaCl solutions were discontinued, and the results obtained were discarded since they did not provide information on the current and potential behaviour at higher electrolyte concentration.

In addition, LPR and MPP tests were carried out on few samples with 100 μm crevice widths immersed in 0.5 M NaCl solution to measure the polarization resistance, R_p , and to obtain the region of passivity along an AISI 304 SS crevice. The information obtained from the LPR and MPP tests were used for the estimation of the rate of corrosion at each location in the crevice. Results from the preliminary tests are presented in the section 4.2.3.

4.2.3 Potentiodynamic Scan and Linear Polarization Results

In this section, the results obtained from the LPR and MPP tests will be discussed. For test Sample C with100 μm crevice width, the LPR scan was done before the long term exposure of the crevice assembly for the MGC test. The galvanic couple was polarized ±20 mV around the open circuit potential (E_{corr}) with a scan rate of 0.167 mV/sec and a sample period of 2 seconds to measure the polarization resistance of the sample. Comparison of the polarization resistance results obtained after the LPR test and the corrosion rate calculation after the MGC test did not show close correlation.

It is expected that the position with the highest corrosion rate will have a lower polarization resistance than the ones with lower corrosion rate, where R_p is inversely proportional to the corrosion rate of a sample (Bard and Faulkner, 1980). However, this was not the case for the different positions along the crevice. Therefore, it was inferred that in a crevice condition, the measured polarization resistance, R_p, values may not be valid because the scan rate creates concentration gradients within the crevice causing the theoretical calculation of the R_p from the Tafel slopes to be erroneous. Table 4.3 shows the polarization resistance values and the corrosion rate obtained for 1 to 6 cm from the crevice mouth of Sample C.

Table 4.3 Comparison of the Polarization Resistance and the corrosion rates for Sample C AISI 304 SS galvanic couple in 0.5 M NaCl solution (crevice width of 100 μm) at room temperature, 6.5 pH and 168 hour of exposure.

Sample tested	Distance from crevice mouth(cm)	R_p (Ohms)	Corrosion rate (mmpy)
C	1	667 300	0.145
	2	805 800	0.012
	4	382.8	0.007
	6	440.3	0.009

The MPP scan was carried out on Sample C1 and D1 with crevice width of 100 μm immersed in 0.5 M NaCl solution. A large potential sweep of -0.2 V to +1.2 V with a scan rate of 3 mV/s and a sample period of 1 second was applied to each sample. This large sweep caused a shift of the potential further away from the OCP of the metal. As a result, the metal surface was altered, and the change in the crevice electrolyte concentration along the crevice affected the polarization curve generated, which showed no passivation behaviour for each location along the crevice.

In addition, the effect of corrosion products generated at the different locations along the crevice may influence the passivation behaviour of the metal. The extrapolation of the linear portion of the cathodic region on the polarization curve for all four locations along the crevice to the corrosion potential to obtain the Tafel slopes was performed internally by the Gamry software. The Tafel slopes obtained were in the acceptable range of ± 100 mV/decade (Frankel, 2008; Bard and Faulkner, 1980). However, the determination of the anodic Tafel slopes near OCP for all four locations

along the crevice was very difficult and inaccurate as compared to the value determined by the extrapolation of the cathodic region. This may be due to the surface changes that occurred in the crevice from the potential sweep in the anodic region. The results obtained from these tests were discarded and further studies were not repeated with this technique, as the preliminary tests did not yield reproducible results.

From the results obtained in this section, it can be inferred that anodic polarization scans that require potential sweep do not yield good results in crevice conditions. This is due to the concentration gradients created in the narrow geometries as a result of the polarizing the sample. At the end of each experiment, physical examination of the tested samples showed tiny pits long the crevice length as will be presented in the section 4.3.

4.3 Surface Morphology Analysis

Surface analysis of the uncoupled crevice components after each experiment was carried out using the inverted microscope with 100 times magnification. Some evidence of localized attack such as micropits was detected at the metal-resin boundary at 1 cm from the crevice mouth in some samples, and at other locations along the crevice. These pits are believed to occur as a result of sulfide inclusions in the metal matrix (Alkire and Lott, 1985).

Figure 4.7 and 4.8 shows that pits are distributed on the metal surface of Sample C at 1 cm and 2 cm from the crevice mouth. The distribution of pits at positions closer to the crevice tip, 4 cm and 6 cm, was few as compared to those observed at 1 cm and 2 cm from the crevice mouth. The pits presented in the figure are shallow with the width

ratio of 100 µm. These shallow pits correspond with the low corrosion rate of 0.145 mmpy and 0.012 mmpy observed at the position 1 cm and 2 cm from the crevice mouth.

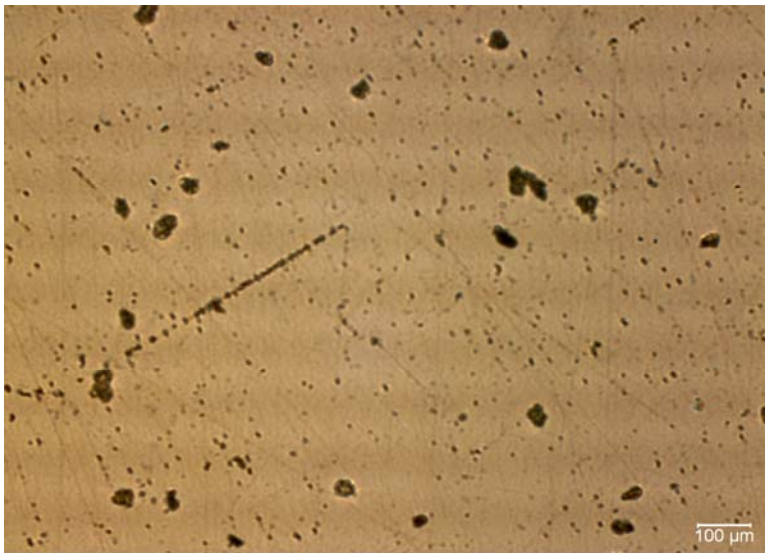

Figure 4.7 Surface morphology of 1cm from the crevice mouth for Sample C.

Figure 4.8 Surface morphology of 2 cm from the crevice mouth for Sample C.

As seen in Figures 4.7 and 4.8, crevice corrosion nucleates by the formation of pits in the crevice region at the initiation of crevice corrosion. Similar observations have

been reported by Simeos and Ferreira, (1987). In summary, this experiment was successful in demonstrating how galvanic corrosion monitoring in a laboratory can provide information on the use of identical metals couple for real-life applications. It is observed that since the metals have same reduction potential on the galvanic series, the presence of a larger cathode area has negligible effect on the corrosion behaviour of the galvanic couple.

For a galvanic couple subjected to crevice conditions, *in situ* measurements of current behaviour within the crevice immersed in a 0.5 M NaCl solution at room temperature has shown that the highest anodic current was observed at the position closest to the crevice mouth. However, the variation in surface inhomogeneities and crevice geometry account for the stochastic nature of crevice corrosion initiation along the crevice. This is in close agreement with the pH profile of previously tested identical AISI 304 SS crevice by Alavi and Cottis (1987), which showed the lowest pH value at locations closest to the crevice mouth.

The corrosion rate calculated from the galvanic current density showed very low corrosion rate values of approximately 0.06 mm/year for the AISI 304 SS crevice coupled to an identical metal bold surface. The linear polarization resistance scan and the potentiodynamic polarization scan did not yield good results under the crevice conditions due to the effects of the concentration gradients in these localized areas.

5 Conclusions and Recommendations

5.1 Conclusions

In conclusion, the results obtained from this study showed that:

1. The experimental cell provided two real time signals for measuring crevice corrosion between a galvanic couple, namely; the current flow between the anodic and the cathodic site, and the potential variation at various locations in the crevice.
2. The sudden increase in corrosion current after the incubation period indicated the initiation and propagation of crevice corrosion. In the event where wide crevice widths were studied, the time of initiation increased as the crevice width increased.
3. The variation in potential along the crevice provided a qualitative signal of localized attack, where potential shift in the noble direction was observed during the incubation period and a shift in the active direction denotes increase in corrosion current. The cathode area to anode area ratio of 2.5:1 had no effect on the metal dissolution rate observed inside the crevice.

5.2 Recommendations

Based on the experimental challenges encountered in the course of this work, the following recommendations are made for future work:

1. The present crevice design as seen in Figure 3.1 and 3.2 should be modified to allow the assessing and measuring of the crevice width created after the coupling of the crevice assembly before and after each experiment. The modification will also help control the problem of short circuiting between the assembly and the Gamry which is a challenge for the present design. In addition, thin AISI 304 stainless steel wires can be used as the working electrode as a modification to the AISI 304 SS 0.65 diameter rod used in the present study.
2. The effect of increased temperature and chloride concentration on the onset and extent of severity of the localized attack at the different locations in the crevice should be studied, for comparison to the results obtained at room temperature and 0.5 M NaCl solution.
3. Time of exposure should be increased for wider crevice width to have an idea of the length of time required for wider gaps to undergo active corrosion.
4. Very large cathode area to anode area ratio of about 10:1 should be studied to observe the effect of large cathode area on the extent of corrosion for an identical metal galvanic couple.
5. The Mott Schottky technique should be used to determine the properties of passive film at the different locations along the crevice, and electrochemical changes that occur on the bold surface of 304 stainless steels during the induction and propagation phases of crevice corrosion.

References

Abdusalem, M. I. (2005). Behaviour of Crevice Corrosion on Iron, Corr. Sc., 47, pp 1336 – 1351.

Abdusalem, M. I. (2007). The Role of Electrolyte Concentration on Crevice Corrosion of Pure Nickel, Mat. & Corr., 58, pp 511-513.

Ahmad, Z. (1994). *Principles of Corrosion Engineering and Corrosion Control*, Butterworth – Heinneman 128, Oxford, UK.

Agarwal, A. S., Landau, U., Shan, X., & Payer, J. H. (2007). Modelling the Effects of Crevice Former, Particulates, and the Evolving Surface Profile in Crevice Corrosion, The ECS Trans., 3, pp 459- 471.

Alavi, A., & Cottis, R. A. (1987). The Determination of pH, Potential and Chloride Concentration in Corroding Crevices on 304 Stainless Steel and 7475 Aluminium Alloy, Corr. Sc., 27, pp 443- 451.

Alkire, R. C., & Siitari, D. (1982). Initiation of Crevice Corrosion: II – Mathematical Model for Aluminium in Sodium Chloride Solutions, J. Electrochem. Soc., 129, pp 488 – 496.

Alkire, R. C., & Lott, S. E., (1985). The Initiation of Crevice Corrosion on Grade 304 Stainless Steel", The Electrochem. Soc., 85, pp 17 – 17.

Alkire, R. C., & Lott, S. E. (1989). The Role of Inclusion on Initiation of Crevice Corrosion of Stainless Steel, J. Electrochem. Soc., 136, pp 973 – 979.

Herbert, K., & Alkire, R. (1983) Dissolved Metals Species Mechanism for Initiation of Crevice Corrosion of Aluminium J. Electrochem. Soc., 130, pp 1007 – 1014.

Arai, Y., Mabuchi, K., Honda, T., Shouji, S., Yokosuka, T., & Takashi, H., (2002). Crevice Corrosion of Type 304L and 316L Stainless Steels in Nitric Acid Solutions, Corr. Eng., 51, pp 217 – 330.

ASTM– G78 – 01, (2007). Standard Guide for Crevice Corrosion Testing of Iron – Base and Nickel – Base Stainless Alloys in Seawater and other Chloride – Containing Aqueous Environments, ASTM International, www.astm.org, (Tue August 4th 2009).

ASTM– G102 – 89, (2004). Standard Guide for Calculation of Corrosion Rates and Related Information from the Electrochemical Measurements, ASTM International, www.astm.org, (Tue August 4th 2009).

Baboian, R. (1976). Electrochemical Techniques for Predicting Galvanic Corrosion, Galvanic and Pitting Corrosion – Field and Laboratory Studies, ASTM STP, 576, pp 5 – 19.

Bard, A. J., & Faulkner, L. R. (1980). *Electrochemical Methods–Fundamentals and Applications*, John Wiley & Sons, New York.

Betts, A. J., & L. H. Boulton. (1993). Crevice Corrosion: Mechanism, Modelling and Mitigation, B. Corr. Journal, 28, pp C256 – C268.

Borex, B., & Olefjord, I. (1985). Preferential Dissolution of Iron during the Polarization of Stainless Steels in Acids, The Inst. Metals, 84, p.134.

Bocher, F., Budiansky, N. D., & Scully, J. R. (2008). Investigation of Crevice Corrosion of AISI 316 Stainless Steel Compared to Ni-Cr-Mo Alloys Using Coupled Multielectrode Arrays. J. Electrochem. Soc., 155, pp 279–295.

ASM International, (1994). Engineering Properties and Service Characteristics in *ASM Specialty Handbook - Stainless Steels 2*, Ed. Davis, J. R.

Corrosion Basic, (2001). NACE Corrosion Costs and Preventive Strategies in the United States, National Association of Corrosion Engineers–Houston, http://events.nace.org/publicaffairs/images_cocorr/ccsupp.pdf (Sun, October 25th 2009).

Chang, H-Y., Park, Y-S., & Hwang, W-S. (2000). Initiation Modelling of Crevice Corrosion in 316L Stainless Steels, J. Mat. Proc. Technol., 103, pp 206 -217.

Chung, H. M., Park, J. H., Ruther, W.E., Sanecki, J. E., Strain, R. V., & Zaluzec, N. J. (1999). Stress Corrosion Cracking of Austenitic Stainless Steel Core Internal Welds, Argonne National Laboratory, pp 1 – 25.

Cho, K., Abdusalem, M. I., & Pickering, H.W., (1998). The Effect of Electrolyte Properties on the Mechanism of Crevice Corrosion in Pure Iron, J. Electrochem. Soc., 145, pp 1862 – 1869.

Chen, Y.Y., Duval, T., Hung, U.D., Yeh, J.W., & Shih, H.C. (2005). Microstructure and Electrochemical Properties of High Entropy Alloys—A Comparison with Type-304 Stainless Steel, Corr. Sc., 47, pp 2257–2279.

Creus, J., Idrissi, H., & Mazille, H., (1997). Galvanic Corrosion Behaviour of Mild Steel, Al, and Ti in 3 % NaCl Solution: Application to PVD Coatings on Steel Substrate, Surf. Eng., 13, pp 415 – 419.

Dayal, R. K., Parvanthavarthini, N., & Gnanamoorthy, J. B. (1983). Measurement of Crevice Corrosion Resistance of Stainless Steels Using a Potentiodynamic Method, B. Corr. Journal, 18, 184 – 186.

Dexter, S. C., & LaFontaine, J. P. (1998). Effect of Natural Marine Biofilms on Galvanic Corrosion, Corr. Sc., 54, pp 851.

Enos, D. G., & Scribner, L. L. (1997). The Potentiodynamic Polarization Scan – Technical Report 33, Solatron Instruments, 2, pp 1 – 19.

Evitts, R., Gad, M. M. A., Watson, M. K., & Posthewhite, J. (1993). Crevice Corrosion of Nickel Alloys at Elevated Temperatures: Experimental and Modelling Studies. NACE Intl., 601, pp 1 – 10.

Evitts, R. W., Watson, M. K., & Postlethwaite, J. (1996). Numerical Simulation of Crevice Corrosion of Titanium: Effect of the Bold Surface, NACE Intl., 121, pp 121 – 132.

Evitts, R. W. (1997). Modeling of Crevice Corrosion, Ph.D Thesis, University of Saskatchewan, Canada.

Fontana, M. G., & Greene, N. D. (1978). *Corrosion Engineering*, Mc Graw Hill, New York, pp 41 – 44.

Fontana, M. G., & Greene, N. D. (1967). *Corrosion Forms in Corrosion Engineering*, Mc Graw Hill, New York, pp 41 – 44.

Frankel, G. S. (2002). Wagner-Traud to Stern-Geary; Development of Corrosion Kinetics, in Corrosion Retrospective, G. S. Frankel, H. S. Isaacs, J. R. Scully, and J. D. Sinclair, Eds., The Electrochem. Soc., New York.

Fushimi, K., Naganuma, A., Azumi, K., & Kawahara, Y. (2008). Current Distribution During Galvanic Corrosion of Carbon Steel Welded With Type 309 Stainless Steel in NaCl Solution, Corr. Sc., 50, pp 903 – 911.

Griess, J. C. (1968). Crevice Solution of Titanium in Aqueous Salts Solutions, Corr., 24, pp 96 – 109.

Hua, P. L. B., & Ives, M. B. (1998). The Galvanic Coupling Approach to Crevice Corrosion, Mat. Sc. Forum, 289, pp 1103 – 18.

Heppner, K. L., Evitts, R. W., & Postlethwaite, J. (2002). Prediction of the Crevice Incubation Period of Passive Metals at Elevated Temperatures: Part I – Mathematical Model, Can. J. Chem. Eng., 80, pp 8497 – 856.

Heppner, K. L., & Evitts, R.W. (2004). Computation of Mass Transport in Electrolytic Systems Discrete and Continuous Dynamical Systems, Series B, 11, pp 29 – 46.

Jones, D. A. (1996). *Principles and Prevention of Corrosion*, 2nd Ed., Simon and Schuster, pp 572.

Jones, D. A., & Greene, N. D. (1969). Electrochemical Measurement of Low Corrosion Rates, Corr., 22, pp 367 – 370.

Kabi, C., Mukherjee, K. P., & Rastogi, M. C. (1985). Effect of Galvanic Coupling on Active – Passive Transition Behaviour of Austenitic Stainless steel, J. Electrochem. Soc. India, 34, pp 256 – 260.

Kain, R. M. (1979). Crevice Corrosion Resistance of Austenitic Stainless Steel in Ambient and Elevated Temperature Seawater, NACE, 79, pp 1 – 18.

Kain, R. M. (1985). Recent Developments in Test Methods for Investigating Crevice Corrosion, ASTM STP, 866, pp 299 – 323.

Kennell, G. F., Evitts, R.W., & Heppner, K.L. (2008). A critical crevice solution and IR drop crevice corrosion model, Corr. Sc., 1, pp 1-10.

Kennell, G. F., & Evitts, R.W. (2009). Crevice Corrosion Cathodic Reactions and Crevice Scaling Laws, Electrochim. Acta, 54, pp 4696-4703.

Klassen, R. D., Roberge, P. R., & Hyatt, C. V. (2001). A Novel Approach to Characterizing Localised Corrosion within a Crevice, Electrochim. Acta, 46, 3705 – 3713.

Kadry, S., (2008) Corrosion Analysis of Stainless Steel, European J. Sc. Research, 22, pp 508 – 516.

Laycock, N. J., Stewart, J., & Newman, R. C. (1997). The Initiation of Crevice Corrosion in Stainless Steels, Corr. Sc., 39, pp 1791 – 1809.

Ling, X., & Ma, G. (2009). Effect of Ultrasonic Impact Treatment on the Stress Corrosion Cracking of 304 Stainless Steel Welded Joints, J. Pressure Vessel Technol, 131, pp 1791 – 1809.

Lee, T. S. (1981). A Method for Quantifying the Initiation and Propagation Stages of Crevice Corrosion, ASTM STP*,* 727, pp 43 – 68.

Lee, T. S., & Kain, R. M. (1983). Factors Influencing the Crevice Corrosion Behaviour of Stainless Steels in Seawater, *National Association of Corrosion Engineers*, 83, pp 1 – 12.

Mansfeld, F. (1976). The Polarization Resistance Technique for Measuring Corrosion Currents, Adv. Corr. Sc. Technol., M. G. Fontana and R. W. Staehle, Eds., Plenum, New York,.

Mckay, P., & Mutton, D.B. (1985). An Electrochemical Investigation of Localized Corrosion on Titanium in Chloride Environments, Corr*., NACE*, 41, pp 52 – 62.

Muwila, A. (2006). The Effect of Manganese, Nitrogen and Molybdenum on the Corrosion Resistance of a Low Nickel (<2 wt %) Austenitic Stainless Steel, M.Sc Thesis, University of the Witwatersrand, Johannesburg.

Mulford, S. J., & Tromans, D. (1988). Crevice Corrosion of Nickel-Based Alloys in Neutral Chloride and Thiosulfate Solutions, Corr. Sc., 44, pp 891.

Na, E., Ko, J., & Baik, S. (2005). Electrochemical Evaluation of Crevice Corrosion of 430 Ferritic Stainless Steel Using the Microcapillary Tube Technique, Corr. Sc., 186, pp 65 – 74.

Jargelius – Patterson, R. F. A. (1999). Electrochemical Investigation of the Influence of Nitrogen on the Pitting Corrosion of Austenitic Stainless Steels, Corr. Sc., 41, pp 1639 – 1664.

Pickering, H.W. (1986). On the Role of Corrosion Product in Local Cell Processes, Corr. Sc., 35, pp 125.

Pickering, H.W., Cho, K., & Nystrom, E. (1993). Microscopic and Local Probe Method for Studying Crevice Corrosion and Its Application to Iron and Stainless Steel, Corr. Eng. Sc. Technol., 35, pp 775 – 783.

Postlethwaite, J., Evitts, R. W., & Watson, M. K. (1995) Modelling the Initiation of Crevice Corrosion of Passive Alloys at Elevated Temperature, NACE Intl., 192, pp 367 – 377.

Oldfield, J. W., & Sutton, W. H. (1978). Crevice Corrosion of Stainless Steel I – A Mathematical Model, B. Corr. Journal 13, pp 13 – 22.

Pickering, H.W. (2003). Important Early Developments and Current Understanding on the IR Mechanism of Localized Corrosion, J. Electrochem. Soc., 150, pp K1–K12.

Popov, B. N., & White, R. E. (1995) Electrochemical and Corrosion Experimental Techniques, Notes USC, pp 1- 25.

Reclaru, L., Lerf, R., Eschler, P.Y., Blatter, A., & Meyer, J. M. (2002). Pitting, Crevice and Galvanic Corrosion of REX Stainless Steel/CoCr Orthopedic Implant Material, Biomaterials, 23, pp 3479 – 3485.

Scully, J. R. (1990). Electrochemical Methods for Laboratory Corrosion Testing, Corr. Test. Evaluation, ASTM Intl., West Conshohocken, PA.

Scully, J. R. (2000). Polarization Resistance Method for Determination of Instantaneous Corrosion Rates, Corr., 56, pp 199–218.

Sedriks, A.J. (1985). Metallurgical Aspects of Passivation of Stainless Steels, Proc. Stainless Steels, 84, pp 125.

Sedriks, A.J. (1986). National Association of Corrosion Engineers, 42, pp 376-389.

Shirazi, M. (1996). Localized Corrosion of Stainless Steel in High Temperature Potash Brine, M.Sc Thesis, University of Saskatchewan, pp 199–218.

Shaw, B. A., Moran, P., & Garland, P. O. (1991). The Role of Ohmic Potential Drop in the Initiation of Crevice Corrosion on Alloy 625 in Seawater, Corr. Sc., 32, pp 707

Shi, G. (1990). Study of Crevice Corrosion of Titanium, M.Sc Thesis, University of Saskatchewan, Canada.

Shreir, L. L., Jarman, R. A., & Burstein, G. T. (1994) *Corrosion- Metal/Environment Reactions*, Butterworth Heinemann, London.

Simoes, A. M. P., & Ferreira, M. G. S. (1987). Some Aspects of the Initiation Phase of Crevice Corrosion of Stainless Steel in Chloride Solution, Key Eng. Mat., 20, pp 3125 – 3128.

Sun, D., Li, T., Yu, H., & Yang, D. (2000). Galvanic Effects on the Electrochemical Behaviours of Bare Surface of 304 Stainless Steel, Trans. Nonferrous Met. Soc. China, 10, pp 253 – 256.

Z. Szklarska-Smialowska. (1986). Pitting Corrosion of Metals, NACE Houston, pp 301.

Trasatti, S. P., & Mazza, F. (1996). Crevice corrosion: a neural network approach, B. Corr. Journal, 31, pp 105 – 112.

Walton, J. C., Cragnolino, G., & Kalandros, S. K. (1996). A Numerical Model of Crevice Corrosion for Passive and Active Metals, Corr. Sc., 38, pp 1 – 18.

Wolfe, R. C., Pickering, H. W., & Shaw, B. A. (2006). Microprobe Study of pH During the Induction Period Preceding Crevice Corrosion, J. Electrochem. Soc., 153, pp B25 – B32.

Xu, Y., Wang, M., & Pickering, H. W. (1995). Potential Distribution, Shape Evolution and Modelling of Pit Growth for Ni in Sulphuric Acid, B. Electrochem. Soc., 142, pp 2986 – 2995.

Walsh, F. (1991). The Overall rates of Electrolytic Reactions: Faraday's Law of Electrolysis, Trans. Inst. Metal Finishing, 69, pp 135 – 157.

Yin, Z. F., Yan, M. L., Bai, Z. Q., Zhoa, W. Z., & Zhou, W. J. (2008). Galvanic Corrosion associated with SM 80SS steel and Ni-based Alloy G3 Couples in NaCl Solution, Electrochim. Acta, 53, pp 6285 – 6592.

Zhu, X. (2005). Study on Galvanic Corrosion of Titanium Alloys in Seawater, *Revue de metallurgie*., 86, pp 667 – 670.

APPENDIX A

Calculation of the Equivalent weight of AISI 304 Stainless Steel

Calculation of the correspondence between the corrosion rate and the anodic current density for an alloy requires a determination of the equivalent weight for the alloy, E_w. This equivalent weight is the weighted average of atomic weight to the ion valence for the major alloying elements in any given alloy, also known as the Molecular weight, M_w, of the alloy (Walsh, 1991).

For an AISI 304 stainless steel with chemical composition as shown in Table A.1, the major alloying elements are as shown in Table A1 (ASTM G102-89).

Table A.1 Equivalent weight for major alloying elements in AISI 304 stainless steel.

Common Designation	UNS	Element w/constant valence	Lowest		Second		Third	
			V.V	E_w	V.V	E_w	E.V	E_w
304	S30400	Ni/2	Fe/2, Cr/3	25.14	Fe/3, Cr/3	18.99	Fe/3, Cr/6	15.72

*V.V is Variable Valence, E.V is the Element Valence and E_w is the Equivalent Weight.

Assumptions:

For the calculation of the equivalent weight of AISI 304 Stainless steel, the corrosion potential in 0.5 M NaCl solution is -220mV SCE.

Composition: Chromium, range of 18-8% - actual 18%

Nickel, range of 8-10% - actual 8%

Iron, Balance (ignoring minor elements)

Chromium and Nickel give 36%, therefore, for an alloy with 100g of elements,

Percentage of Iron = 100 – 26 = 74%.

Recall valence values (V.V) from Table A1 where

Chromium: +3

Nickel: +2

Iron: +2

Calculations: Assuming 100g of alloy dissolved, therefore, the gram equivalents of the dissolved components are given by the sum of the fractional number of equivalent for each alloying elements Chromium, Nickel and Iron, Q:

$$Q = \frac{18}{51.996} \times 3 + \frac{8}{58.71} \times 2 + \frac{74}{55.847} \times 2 \quad \text{(A.1)}$$

$$Q = 1.039 + 0.273 + 2.650 \quad \text{(A.2)}$$

$Q = 3.962$ gram equivalent

Therefore, the alloy equivalent weight, E_w , is given by

$\frac{100}{3.962} = 25.24$ g/equivalent.

APPENDIX B

Calculation of the Corrosion Rate of an AISI 304 Stainless Steel

From the anodic current values obtained from the galvanic corrosion (MGC) tests, the anodic current density was calculated using the anode area (0.31 cm^2) to for all positions along the crevice. The anodic current densities were used for the calculation of the rate of corrosion at the different locations along the crevice. It is worthy to note that the corrosion rate is not only related to the current density, i_{corr}, but a function of the atomic-fraction-weighted-values of the atomic weight, ion valence and density of the alloy (Chen *et al.* 2005).

The value of the corrosion rate can be estimated according to Faraday's law (Bard and Faulkner, 1980):

$$\text{Corrosion rate (mm/py)} = \frac{M_w \mathrm{I}_{corr}}{ZFA\rho} \quad \text{(B.1)}$$

$$\text{Corrosion rate (mm/py)} = M_w \mathrm{i}_{corr} \times (207.8) \quad \text{(B.2)}$$

where M_w is the molecular weight of metal (g/mol), I_{corr} is the corrosion current calculated from the experiments, i_{corr} is the corrosion current density in μA/ cm^2, Z is the number of electrons transferred during electrochemical reaction, F is the Faraday constant (96,487C.mol^{-1}), A is the area of the working electrode (cm^2) and ρ is the density of the metal (g/cm^3).

For corrosion rate of all samples studied;

ANODE AREA, Z	0.31	cm^2
FARADAY CONSTANT,F	96500	C/mol

NO OF ELECTRONS,Z	2	
MOLECULAR WEIGHT, M_w	25.24	g/mol
DENSITY, ρ	7.87	g/cm^3

Table B1 Corrosion rate calculation for samples with crevice widths **100 μm to 600 μm** immersed in 0.5 M NaCl solution at room temperature and pH of 6.5.

Crevice Width(μm)	Test Duration	Sample	Distance from crevice mouth (cm)	I_{corr} (μA)	i_{corr} (μA/cm^2)	Corrosion Rate (mm/yr)
100	24	A	1	-2.87×10^{-8}	-9.23×10^{-8}	-0.000485
			2	-2.84×10^{-8}	-9.17×10^{-8}	-0.000481
			4	-2.92×10^{-8}	-9.41×10^{-8}	-0.000494
			6	-2.75×10^{-8}	-8.87×10^{-8}	-0.000465
100	**168**	**B**	**1**	**3.984**	**1.29×10^{-5}**	**0.0674**
			2	-3.22×10^{-8}	-1.04×10^{-7}	-0.000546
			4	-2.97×10^{-8}	-9.59×10^{-8}	-0.000503
			6	-2.54×10^{-8}	-8.19×10^{-8}	-0.000430
200	24	1	1	-8.97×10^{-9}	-2.89×10^{-8}	-0.000152
			2	-2.90×10^{-8}	-9.34×10^{-8}	-0.000490
			4	-3.06×10^{-8}	-9.87×10^{-8}	-0.000518
			6	-2.89×10^{-8}	-9.33×10^{-8}	-0.000489
300	24	2	1	-8.37×10^{-9}	-2.70×10^{-8}	-0.000142
			2	-3.30×10^{-9}	-1.06×10^{-8}	-5.58×10^{-5}
			4	-3.30×10^{-9}	-1.06×10^{-8}	-5.57×10^{-5}
			6	-3.72×10^{-9}	-1.20×10^{-8}	-6.29×10^{-5}
400	24	3	1	-1.90×10^{-8}	-6.12×10^{-8}	-0.000321
			2	-2.64×10^{-8}	-8.51×10^{-8}	-0.000446

			4	-3.34×10^{-9}	-1.07×10^{-8}	-5.66×10^{-5}
			6	-2.85×10^{-8}	-9.21×10^{-8}	-0.000483
500	24	4	1	-3.12×10^{-8}	-1.01×10^{-7}	-0.000527
			2	-7.36×10^{-9}	-2.38×10^{-8}	-0.000125
			4	-1.03×10^{-8}	-3.33×10^{-8}	-0.000175
			6	-2.85×10^{-8}	-9.50×10^{-8}	-0.000498
600	24	5	1	-1.98×10^{-9}	-6.38×10^{-8}	-0.000335
			2	-2.59×10^{-8}	-8.35×10^{-8}	-0.000437
			4	-4.80×10^{-9}	-1.55×10^{-8}	-8.11×10^{-5}
			6	-1.25×10^{-9}	-4.02×10^{-9}	-2.11×10^{-5}

*Bold result with highest corrosion rate at 1 cm from the crevice mouth for Sample B.

Table B2. Corrosion rate calculation for samples with crevice widths **100 μm** immersed in 0.5 M NaCl solution at room temperature and pH of 6.5.

Test Duration(Hours)	Sample	Distance from crevice mouth (cm)	I_{corr} (μA)	i_{corr} (μA/cm^2)	Corrosion Rate (mm/yr)
168	**C**	**1**	**8.593**	**2.77×10^{-5}**	**0.1454**
		2	-3.05×10^{-8}	-9.84×10^{-8}	-0.000516
		4	-2.74×10^{-9}	-8.84×10^{-8}	0.000463
		6	-3.99×10^{-8}	-1.29×10^{-7}	-0.000677
168	**D**	1	-3.59×10^{-8}	-1.20×10^{-7}	-0.000608
		2	-3.29×10^{-8}	-1.06×10^{-7}	-0.000557
		4	-1.25×10^{-8}	-4.02×10^{-8}	-0.000211
		6	**0.6951**	**2.24×10^{-6}**	**0.0118**
168	**E**	**1**	**0.3844**	**1.24×10^{-6}**	**0.00650**
		2	4.36×10^{-7}	1.41×10^{-6}	0.00738
		4	-3.42×10^{-8}	-1.02×10^{-7}	-0.000578
		6	3.04×10^{-8}	9.80×10^{-8}	0.000513
168	**F**	**1**	**0.5204**	**1.68×10^{-6}**	**0.00880**
		2	-3.35×10^{-8}	-1.08×10^{-7}	-0.000567
		4	-4.45×10^{-9}	-1.44×10^{-8}	-7.53×10^{-5}
		6	-2.88×10^{-8}	-9.29×10^{-8}	-0.000487

* Bold result with highest corrosion rate at 1 cm from the crevice mouth for Samples C to F, with exception of D showing highest corrosion at 6 cm from the crevice mouth.

Table B3 Corrosion rate calculation for samples with crevice widths **100 μm** immersed in 0.5 M NaCl solution at room temperature and pH of 6.5 continue.

Test Duration(Hours)	Sample	Distance from crevice mouth (cm)	I_{corr} (μA)	i_{corr} (μA/cm^2)	Corrosion Rate (mm/yr)
168	**G**	**1**	**3.705**	**1.20×10^{-5}**	**0.0627**
		2	-3.61×10^{-9}	-1.17×10^{-8}	-6.11×10^{-5}
		4	-3.57×10^{-8}	-1.15×10^{-7}	-0.000603
		6	-3.53×10^{-8}	-1.14×10^{-7}	-0.000598

* Bold result with highest corrosion rate at 1 cm from the crevice mouth for Sample G.

APPENDIX C

Appendix C1: Current variation in crevice with 100 µm crevice width

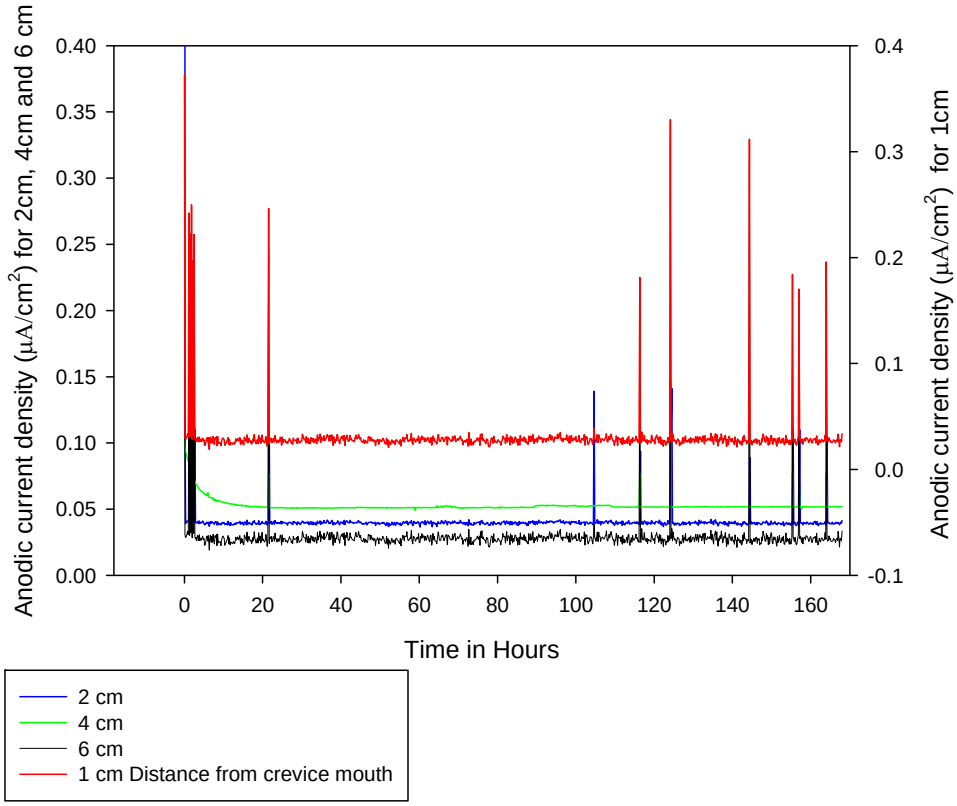

Figure C.1.1 Galvanic current behaviour along AISI 304 SS crevice (Sample E) with 100 µm gap for 168h at pH of 6.5 and room temperature in 0.5 M NaCl solution.

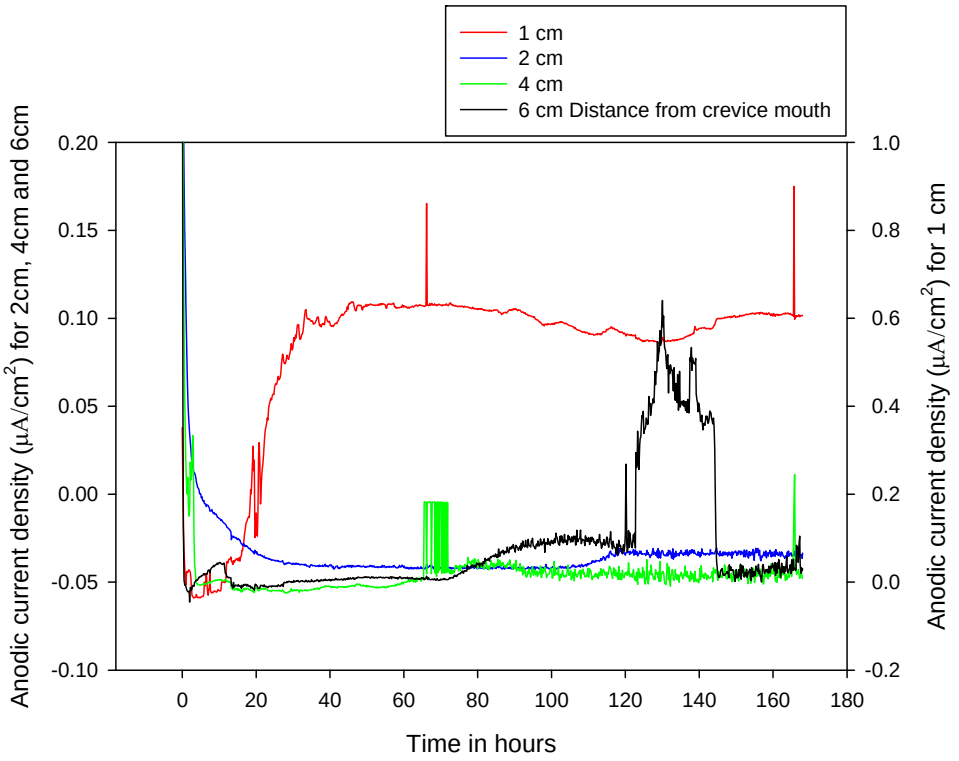

Figure C.1.2 Galvanic current behaviour along AISI 304 SS crevice (Sample F) with 100 μm gap for 168h at pH of 6.5 and room temperature in 0.5 M NaCl solution.

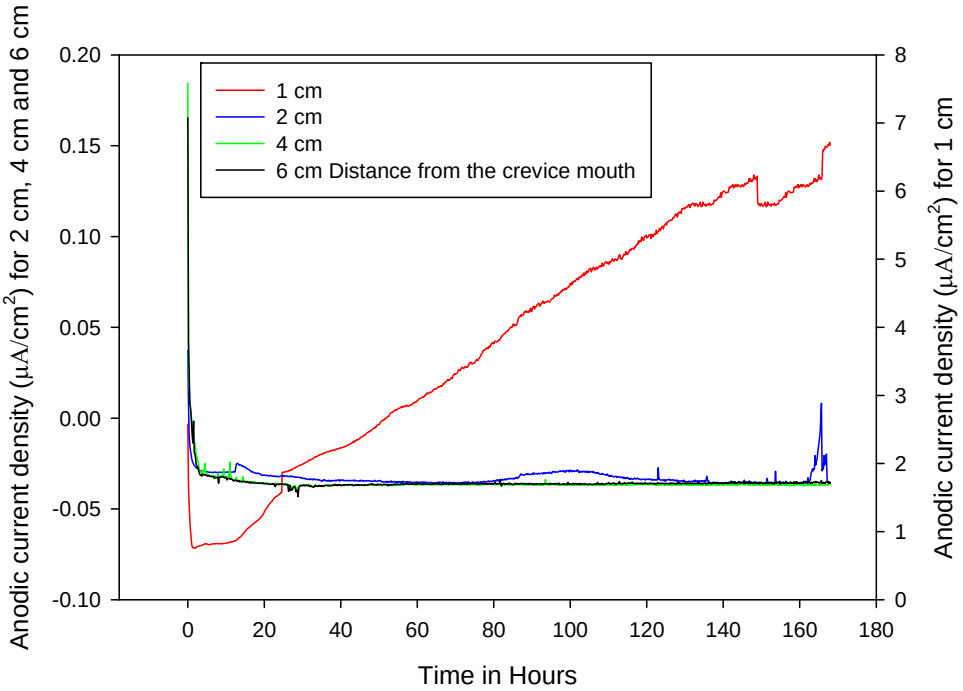

Figure C.1.3 Galvanic current behaviour along AISI 304 SS crevice (Sample G) with 100 μm gap for 168h at pH of 6.5 and room temperature in 0.5 M NaCl solution.

Appendix C2: Potential variation in crevice with 100 µm crevice width

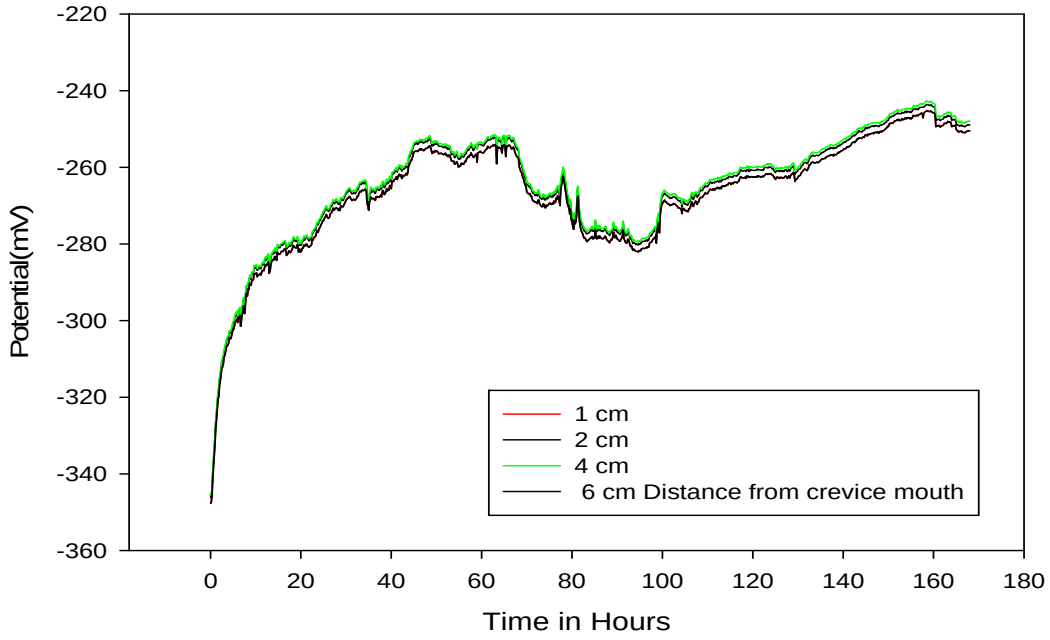

Figure C.2.1 Variation of potential with time along the AISI 304 SS crevice (Sample D) with 100 µm gap for 168h at pH of 6.5 and room temperature.

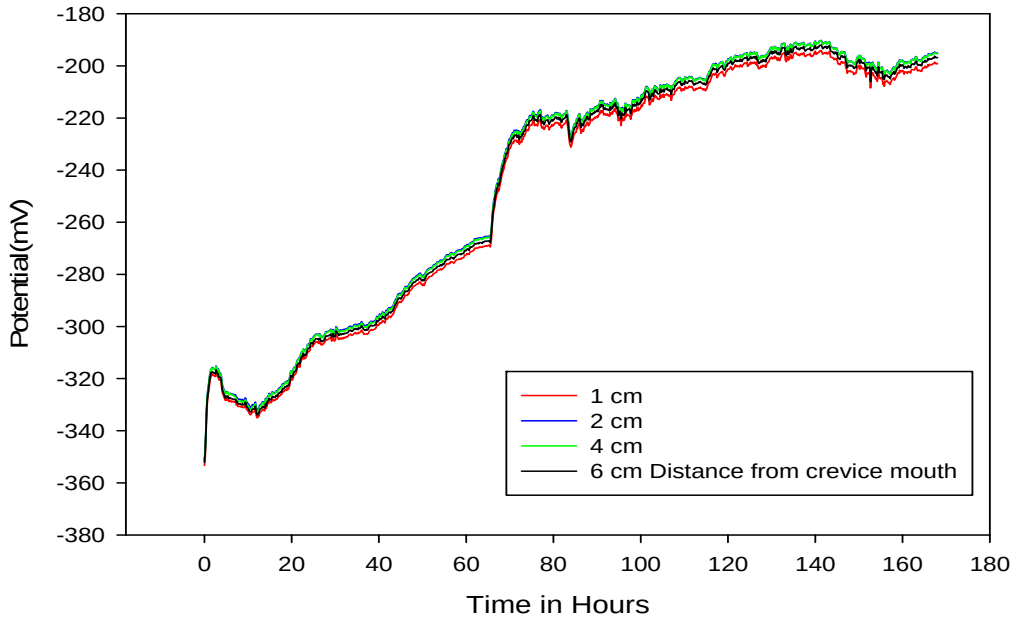

Figure C.2.2 Variation of potential with time along the AISI 304 SS crevice (Sample E) with 100 µm gap for 168h at pH of 6.5 and room temperature.